EXPERIMENTAL STUDY OF PRESSURE SWIRL ATOMIZERS FOR LEAD OXIDE PRODUCTION

by

Nate Byerly

A Thesis

Submitted to the Faculty of Purdue University

In Partial Fulfillment of the Requirements for the degree of

Master of Science in Aeronautics and Astronautics

School of Aeronautics & Astronautics

West Lafayette, Indiana

May 2019

THE PURDUE UNIVERSITY GRADUATE SCHOOL
STATEMENT OF COMMITTEE APPROVAL

Dr. Stephen Heister, Chair
School of Aeronautics and Astronautics
Dr. Sally Bane
School of Aeronautics and Astronautics
Dr. Carson Slabaugh
School of Aeronautics and Astronautics

Approved by:
Dr. Thomas Shih
Head of the Graduate Program

ACKNOWLEDGMENTS

I would first like to thank my advisor Dr. Stephen Heister, without whom I wouldn't have had the chance to do this research. His guidance over the past few years was as necessary to the completion of this thesis as any experiment I did.

The people of Hammond Group Inc. also deserve my thanks for all the time and money they spent to assist me in the completion of this research. Special thanks to Terry Murphy, Peter Wilke and Philip Kowalski for their instruction and guidance throughout the past few years. You were all wonderful people to work with, and I am glad you decided to fund this project. I hope my work will benefit the company in the future.

I would also like to thank my parents who have supported me throughout all of my education and backed me on every good and bad decision I have made over the past few years.

A big thanks goes out to all my friends who went through this process with me. I'll never forget all the gallons of coffee we drank and the late nights in the lab. Having you all go through this program with me was worth more moral support than any words.

Finally, I would like to thank all the professors I have had during my time at Purdue. Everything you taught me has helped me to get where I am today.

TABLE OF CONTENTS

LIST OF TABLES

LIST OF FIGURES

ABSTRACT

Author: Byerly, Nate, A. MSAAE
Institution: Purdue University
Degree Received: May 2019
Title: Experimental Study of Pressure Swirl Atomizers for Lead Oxide Production
Committee Chair: Dr. Stephen Heister

In this experiment, swirl injectors were designed and tested to validate their use in spraying liquid lead into a Barton pot combustion chamber to produce lead oxide at a smaller particle size than the current stream injection. Testing was done with water and air to determine the best design for atomization results, and then the injector was fabricated for liquid lead testing. Thermochemistry calculations showed that due to lead oxidation being a surface reaction, the combustion process was diffusion controlled. These conditions were used to determine residence time inside a Barton pot combustion chamber for predicted droplet sizes. Results of the liquid lead testing showed that final lead oxide particle size and residence time was reduced when using a swirl atomizer in place of a steady feed stream. Further calculations were done to create a model for a standard combustion chamber and injection system for lead oxide production.

CHAPTER 1. INTRODUCTION

1.1 Background

Lead oxide is used in many industrial applications. Its main application is lead acid batteries in which its function is energy storage. Lead acid batteries power almost every car currently on the market. These batteries are formed by mixing partially oxidized lead oxide with water and sulphuric acid [4]. This creates a paste which is pressed into plates and cured. During the curing process, the portions of the lead oxide that haven't been oxidized yet, or "free lead", oxidize and bond the paste onto the plate. The plates are then assembled into batteries.

Lead batteries are still a very large part of the battery market due to the individual cells of the battery having a large power to weight ratio. They are low cost to manufacture and are 98% recyclable [7]. With a global market turnover of about 15 billion dollars a year [5], even a small improvement in the production process for these batteries could yield high profits for manufacturers. Compared to Lithium-ion or Sodium-sulfer, lead acid batteries have similar lifespans, life cycles, and energy efficiencies, while being much cheaper, recyclable, and safer to produce and operate. Although unlike batteries that use raw components, lead oxide must be manufactured.

1.2 Lead Oxide Barton Process

The current process for creating lead oxide is using a Barton reactor [7]. In this process liquid lead is pumped into a large basin. The lead is atomized through contact with a rotating propeller at the bottom of the Barton pot. Additional atomization is achieved through the lead droplets contact

with a baffle plate inside the Barton pot. The temperature of the reactor is controlled through the injection of water. Residence time of lead particles inside the Barton pot is on the order of seconds. Once the particles are oxidized they leave the Barton pot through an air duct on top of the combustor.

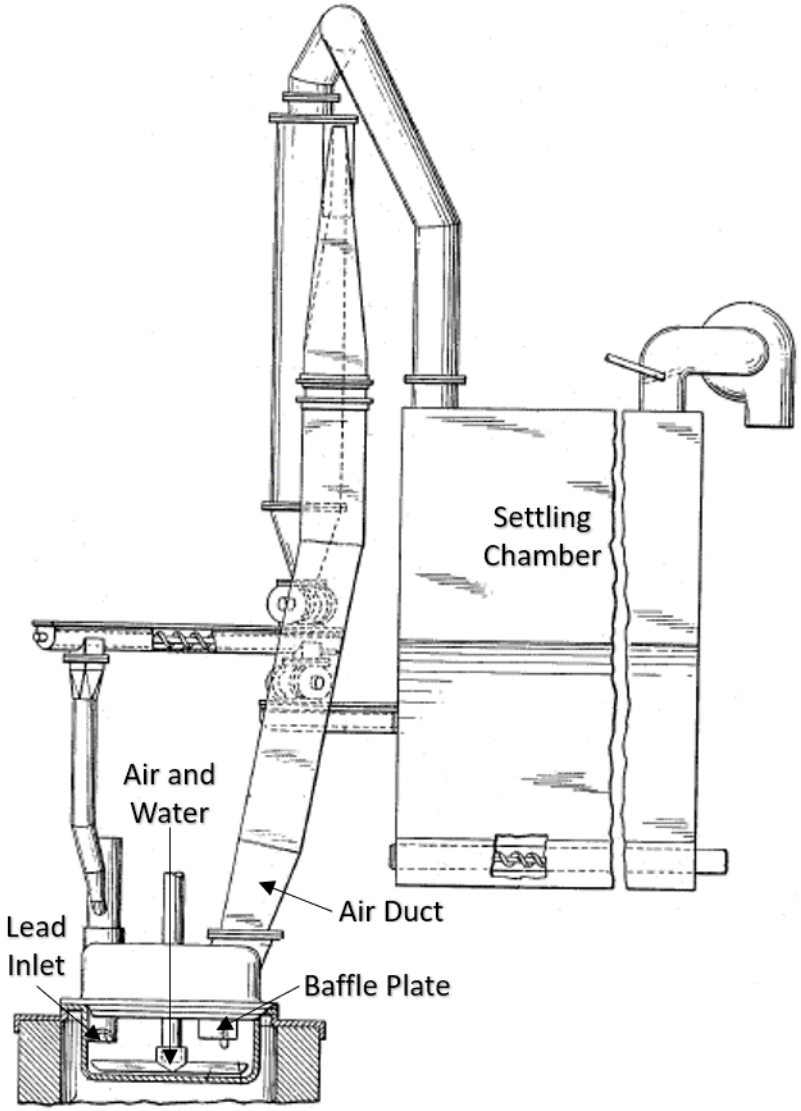

Figure 1.1 Barton Pot System [8]

Figure 1 above shows the entire Barton system. Lead is injected into the combustor in the bottom left corner of Figure 1. The combustor is approximately six feet wide and four feet tall. The blade spins and produces an air current that breaks up the lead into droplets. The blade then whips the lead into the baffle plate. Air and water enter the Barton pot through the blade shaft. Air is provided for combustion and the water is added to control the temperature of the reaction. The air exits out of the duct as shown. The droplets stay in the Barton pot until they have broken up enough to be carried out of the system by the air. The duct then takes these particles of lead oxide into the settling chamber to be collected. The residence time, or the time the lead spends in the Barton pot, is estimated to with the volumetric airflow. It is assumed the lead stays in the Barton pot for the same length of time the air does. The current residence time is approximately a second.

After the particles are collected from the settling chamber, they must be milled to fit product specifications. For lead acid batteries the desired particle size is 1-10 microns in diameter. The particles that exit the Barton pot can be much larger than this and thus require a milling step. One goal of increasing the atomization inside the Barton pot is to remove the need for this step.

1.3 Lead Oxide Chemical Properties

Lead oxide has two crystal structures: α-PbO which is a tetragonal crystal and β-PbO which is an orthorhombic crystal [9]. The tetragonal variation is called “litharge” and is the desired product for energy storage. At combustion temperatures under 912 degrees Fahrenheit litharge is formed. At higher combustion temperatures orthorhombic crystals are formed. Since the adiabatic flame temperature of lead combustion is 2900 F, water is added to the system to ensure the temperature does not go over the transition point from tetragonal to orthorhombic crystal structure. Not much

is known about the combustion of lead which is why a portion of this project was focused on examining the thermochemistry behind the reaction.

Existing thermochemistry data on lead oxidation is scarce and does not cover a large range of temperatures. One piece of existing literature on lead oxidation shows oxidation rates up to 1000°F. The oxidation rate is given as a change in mass over time to show oxide accumulation. These rates are based off of a flat surface of lead oxidizing [9]. For the kinetic oxidation rates used later in this report, the rates are assumed to be able to be applied to droplet oxidation by using the mass of the droplet and surface area of the droplet for the most accurate estimation.

1.4 Operational Parameters

For ideal performance, particle sizes should be in the range of 1-10 microns in diameter. The percentage of oxide in a product varies greatly with its desired use. The range of percent oxide varies from 65 to 95 [1]. Percent oxide refers to the amount of product that is lead oxide with the remaining percent of product being un-oxidized lead or "free lead". This is arguably the most important quality of lead oxide as it controls the energy storage potential in any lead acid battery.

In order to achieve particle size requirements, a milling process is used on the oxide after it leaves the Barton reactor [1]. This process could be removed if the particles coming out of the Barton reactor were small enough to pass under the 10 microns specification. The current method of injecting lead into the Barton reactor is through a channel on the side of the reactor. The lead flows through the channel as a stream into the reactor. This stream is atomized through the aforementioned blade and baffle within the Barton.

1.5 Previous and Current Work

Previous work by Purdue sought to improve the atomization of the Barton pot in order to no longer require the lead oxide to be milled at the end of the process. Work by Rohan Dudaney and Dr. Stephen Heister was done to attempt to atomize the lead prior to its injection into the Barton. Lead and air was pumped through a shear coaxial injector instead of just being pouring into the Barton. The final results of the project was an injector that relied on heated air and room temperature air being pumped through a manifold. The heat exchanger that was supposed to supply the heated air could not be constructed so the system ran off of room temperature air only. When installed, the shear coaxial injector did not provide significant enough improvement to the atomization to remove the milling step.

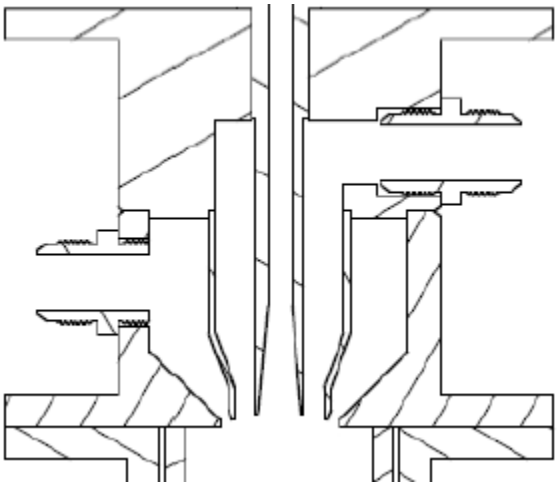

Figure 1.2 Shear Coaxial injector designed by Rohan Dudaney and Dr. Stephen Heister [2]

In Figure 2, the central channel brought the liquid lead into the injector. The inner air manifold was designed for heated air to keep the lead in its liquid state, and the outer air manifold was to bring enough air for oxidization without requiring all of the air to be heated. The rest of this paper is dedicated to the work following this injector design. Two other designs are explored: pintle injectors and pressure swirl injectors. A pintle injector is a tube with small orifices drilled

circumferentially for fuel spray. A swirl injector is a small chamber with tangential inlets that swirl a fluid and uses centrifugal force to spray a liquid.

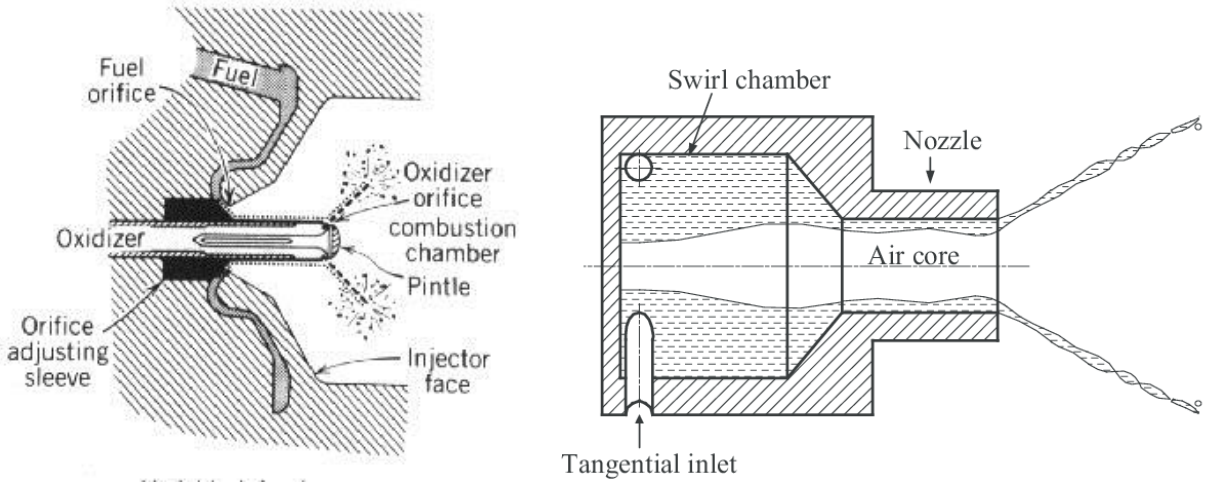

Figure 1.3 Pintle and Swirl Injector Schematics [3], [10]

The objectives of this research were to continue to evolve lead injector designs that could deliver desired atomization characteristics with reasonable/acceptable energy efficiency. To achieve the latter goal, it is desired to limit the amount of high pressure air that might be required and that led the group to consider the pressure swirl and pintle designs shown in Fig. 3. Chapter 2 discusses the design process for the injectors studied. Chapter 3 presents the thermochemistry modeling and estimations used for burn rates. Chapter 4 looks at the possible benefits and the design of a new combustion system. Conclusions and recommendations for future work are provided in Chapter 5.

1.6 Chapter 1 References

[1] Dix, J. E. “A Comparison of Barton-Pot and Ball-Mill Processes for Making Leady Oxide.” *Journal of Power Sources,* 19 (1987): 157-161.

[2] Dudaney, R., Heister, S. “Design and Fabrication of Novel Lead Oxide Combustion Injector.” April, 2017.

[3] Fischer, D. “Pintle Injector Rocket Engines.” *National Space Society.* August 1, 2010. https://space.nss.org/pintle-injector-rocket-engines/.

[4] Kelley, Barry P. “Lead-Acid Battery Manufacture.” *ILO Encyclopaedia of Occupational Health and Safety,* 16 Mar. 2011, www.iloencyclopaedia.org/component/k2/item/661-lead-acid-battery-manufacture.

[5] Linden, David; Reddy, Thomas B., eds. (2002). *Handbook Of Batteries* (3rd ed.). New York: McGraw-Hill. p. 23.5. ISBN 0-07-135978-8.

[6] Sudarsan, V. “Lead Oxide.” *Science Direct*, Elsevier B.V., 2012, www.sciencedirect.com/topics/chemistry/lead-oxide.

[7] “Sustainability of Lead Acid Batteries.” *Hammond Group Inc.*, www.hmndgroup.com/sustainability/.

[8] Vahrenkamp, G., Manor, S., & Coppersmith, F.; National Lead Company, assignee. Process for Producing Lead Oxides. *U.S. Patent No. 3,322,496.* May 30, 1967.

[9] Weyand, Thomas E., "The oxidation kinetics of liquid lead and lead alloys" (1970). *Doctoral Dissertations*. 2042. http://scholarsmine.mst.edu/doctoral_dissertations/2042.

[10] Yang, L., Fu, Q., Du, M. “Atomization of Gelled Propellants from Swirl Injectors with Lead Spring in Swirl Chamber.” *Atomization and Sprays.* January 2011.

CHAPTER 2. INJECTOR DESIGN

2.1 Pintle Injector Design

The shear coaxial injector elements investigated in the early part of the effort create high power demands from compressed airflow and atomization results that were not promising [2]. As a result, Hammond Corp. suggested the swirl injector as a potential candidate. The natural thinning of a swirling film as it expands radially is a highly efficient mechanism for low-power atomization. This style of injector element was developed in the Soviet Union as early as the 1950's for use in rocket injector applications. Given the volume flows of the lead in the desired application are similar to rocket injectors, it does make good sense to evaluate this technology.

Another rocket injector called the pintle was also evaluated [3]. Pintle injectors feature the interaction of a thick film of one fluid, which flows axially along the cylindrical pintle body, with radial jets of the other fluid that flow from a cavity within the pintle itself. This model of injector was tested due it having better atomization properties than a shear coaxial injector and the variability in its design. Although the pintle injector performs well in atomization tests, the required small injection holes ultimately made it unsuitable for lead injection. The beginning of this chapter describes the pintle injector tests and why it was not selected as the final design.

The injector design revolved from the desired flow conditions. The Barton pot runs through 4000-6000 lbs of lead per hour. To ensure that the injector was able to handle the upper limit, each injector was designed with a 6000 lbs per hour flowrate being the optimal run condition. At this point in the project the lead was still fed into the Barton pot using the pressure generated from the

weight of the lead in the pipes or the head pressure of the lead. Therefore, the injector was designed with the objective of minimizing the feed pressure and to use this parameter to increase/vary the flowrates. At the head pressures of around 10 psi, the lead would only be flowing at approximately 12 feet per second. With a pintle injector, the atomization occurs from the air crossflow breaking up the streams of lead instead of the streams breaking up themselves. Since at this point in the experiment a lead pump was not available, it made the pintle an attractive choice. The following figure shows the first iteration of pintle designs tested.

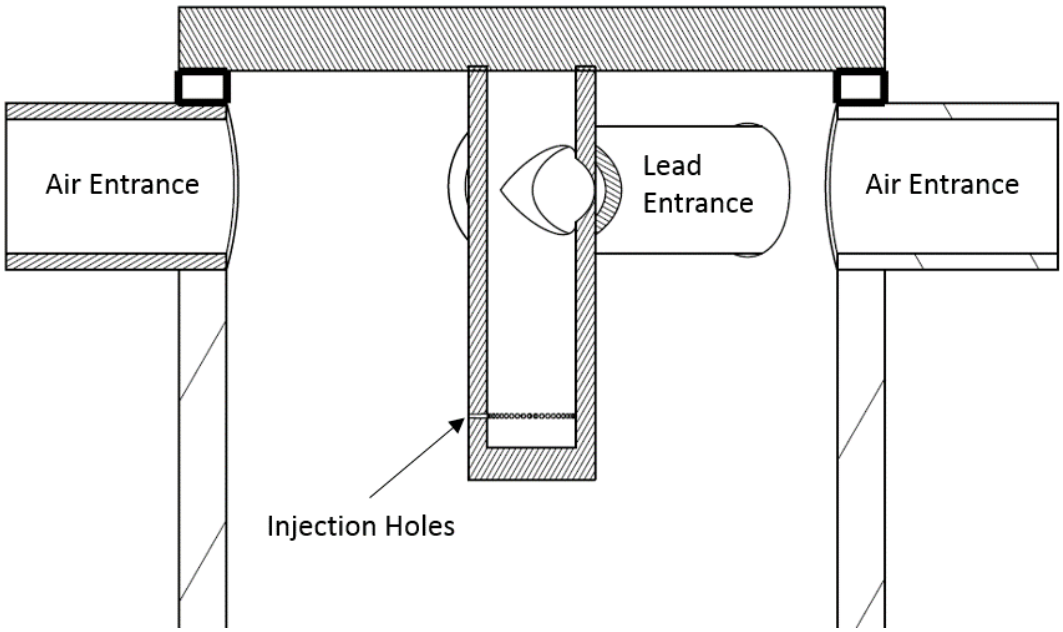

Figure 2.1 Pintle Injector

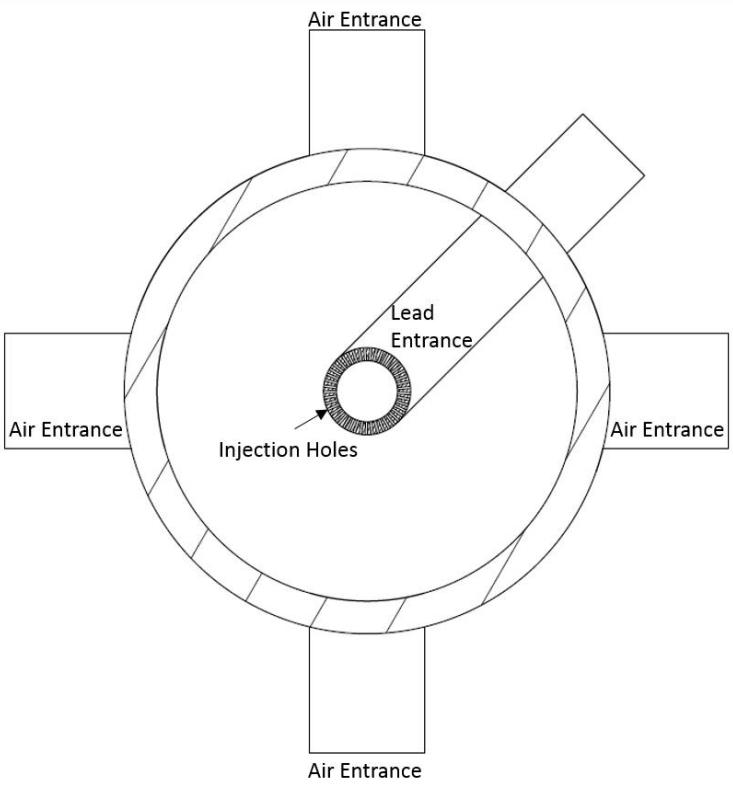

Figure 2.2 Pintle Injector Flat Cross Section

Three variations of the pintle injector were designed: a classic pintle, a classic pintle with a torch through the center, and an inverse pintle injector. The classic pintle was the first design, shown above in Figures 2.1 and 2.2. Using the desired flowrate of 6000 lbs per hour along with a lead speed, v, of 12 feet per second, the following calculations provided the initial sizes of the injector.

$$A = \frac{\dot{m}}{C_d \rho v} \tag{2.1}$$

Using Equation 2.1 to solve for the flow area A, along with an average estimated discharge coefficient C_d of 0.7, the required flow area comes out to 0.043 in^2. The next step is choosing a pintle diameter and a blockage factor. A blockage factor is a dimensionless number that relates the amount of circumference of the pintle is dedicated to injection sites. For a blockage factor of 0.3, 30 percent of the pintle circumference is openings for fuel flow. For an initial design a blockage

factor of 0.5 was selected. This blockage factor was selected because it ends up yielding an appropriate amount of pintle holes [3]. The following equations size the pintle holes using a pintle diameter of 1 inch.

$$A = \frac{\pi n}{4} d^2 \tag{2.2}$$

In Equation 2.2, n is the number of injection sites on the pintle and d is the diameter of those injection sites. Using the blockage factor of 0.5, Equation 2.3 relates the hole diameter, number of holes, and pintle diameter D.

$$\frac{dn}{BF} = \pi D \tag{2.3}$$

Solving for d and substituting into Equation 2.3 into Equation 2.2 gives a relation to relate pintle diameter with the number of holes.

$$A = \frac{\pi n}{4}\left(\frac{BF\pi D}{n}\right)^2 = \frac{\pi}{4n}(BF\pi D)^2 \tag{2.4}$$

Using the pintle outer diameter of 1 inch and the flow are of 0.043 in^2, the required number of holes comes out to 45. Plugging this into Equation 2.3 gives the injection site diameter d as 0.035 in. While this small diameter might work for a regular propellant, lead will not flow through such a small channel. The blockage factor and number of holes can be changed to allow for a larger hole diameter. Decreasing the diameter of the pintle or the blockage factor will increase the hole diameter. Decreasing pintle diameter will not work as the pintle would become too small and the lead inside would become vulnerable to freezing if it is too thin. The only other option is decreasing the blockage factor. This is not ideal either as once the blockage factor gets small enough, the majority of the air will not be impinging the streams of lead. This would raise the need for additional air flow in order to ensure the air that was impinging the lead would have enough velocity to break up the lead. Increasing the amount of air would increase the operational costs as

well. These factors combined gave evidence that a regular pintle injector was not the optimal design. Trying to modify the pintle, a central torch channel was added.

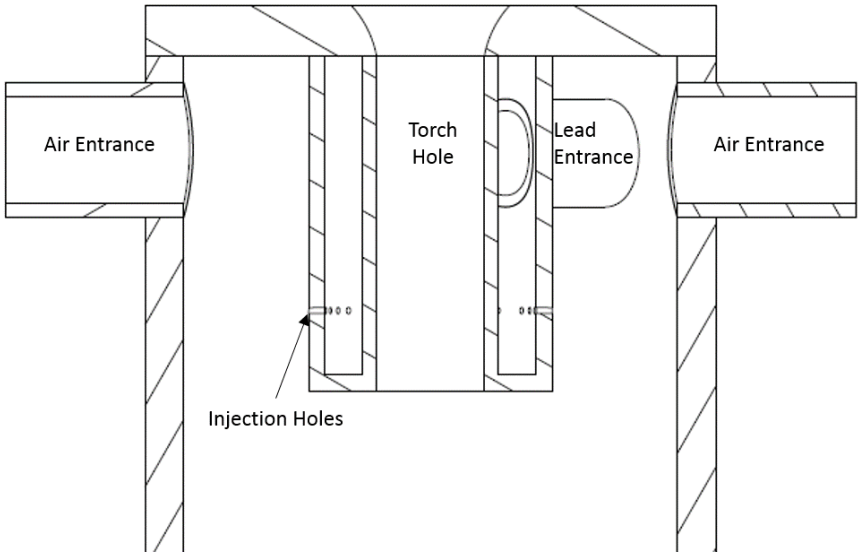

Figure 2.3 Pintle with Center Torch

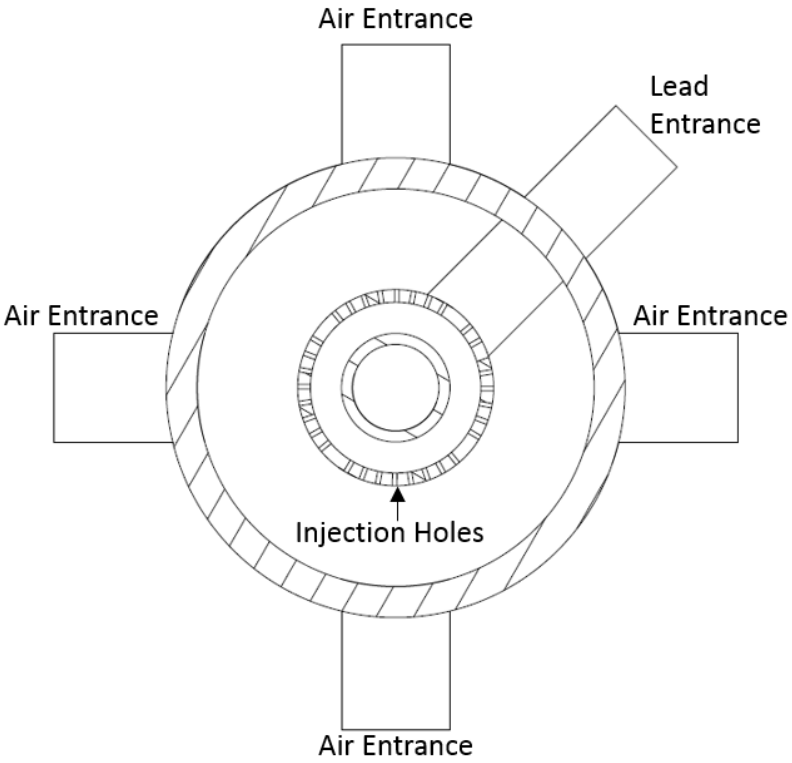

Figure 2.4 Pintle with Center Torch Cross Section

Figures 2.3 and 2.4 show the pintle with an added torch hole. A simple methane torch would be placed above the pintle and guide the flame through the hole. The torch hole was added for a few reasons. The first reason is that a torch would increase the temperature of the reaction zone. This would promote oxidation of the lead immediately upon exiting the pintle. A secondary benefit of the torch was that it kept the lead warm to prevent freezing inside the pintle.

Adding the torch hole also increased the diameter of the pintle without increasing the amount of volume the lead would have to occupy. Because of this, it would have made the injection sites even smaller at a blockage factor of 0.5 so the blockage factor was reduced to 0.4. Also, an injection site was taken out in between the air entrances. This allowed the other injection sites to have a larger diameter and was done because the way air was brought in, those locations would have the smallest air velocity and thus the worst atomization. However, even with the addition of these modifications, the injection sites still remained small enough to cause flow issues. To try and reduce the number of injection sites, a novel inverse pintle design was created. The concept of the inverse pintle is spraying the working fluid from the outside in, instead of the inside out. Figures 2.5 and 2.6 show this in greater detail.

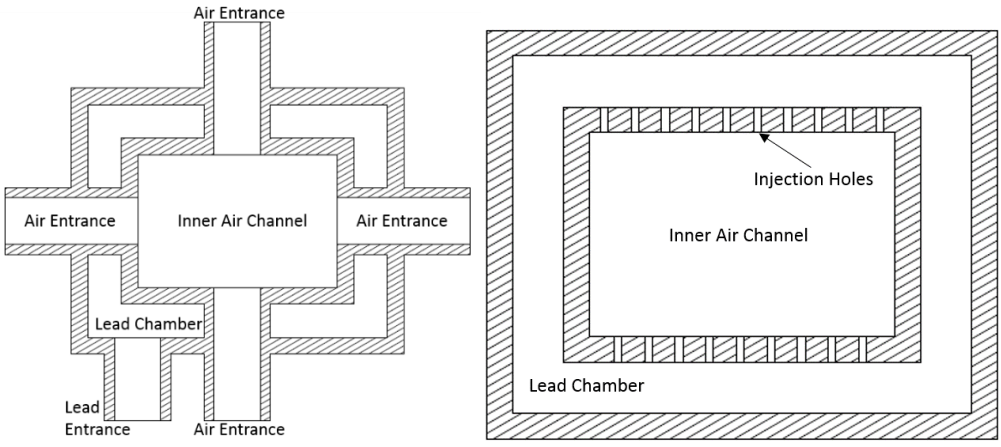

Figure 2.5 Inverse Pintle Design

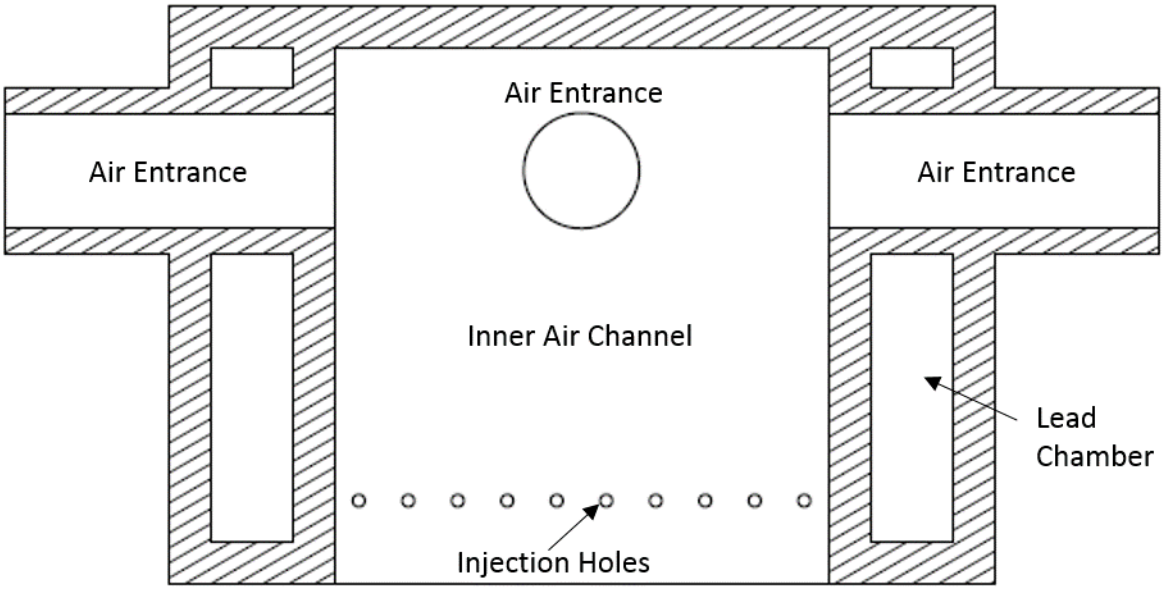

Figure 2.6 Inverse Pintle Cross Section

For the reverse pintle design shown above, the injector would have a central channel of air flowing and injection sites along the walls would spray lead into the air channel. The channel of air was designed to be rectangular. This would allow for injection holes to only be on two sides of the rectangle while still making use of all the air flow. With holes only on two sides, the total number of holes could be reduced while keeping the blockage factor the same.

One drawback to this idea was that the jets of lead would be spraying towards each other. If the lead pressure was raised enough, the jets could impinge which could cause the droplets to combine together leading to larger droplets. The lead could also splash droplets onto the sides of the inner channel where they have the potential to freeze. After working with lead it is safe to assume that if you give it the potential to freeze, it will. One positive factor of this idea is that the lead would be pumped into a large manifold around the injector to feed all of the injection inlets. This would

keep the injector warm and help to prevent freezing of the lead as it flowed through the injection sites.

After evaluating the inverse pintle, the drawbacks outweigh the benefits of the design. The injection inlets, while larger than those on the regular pintle, were still too small for lead to flow freely through. Since this injector is a novel concept, it is also unknown what the spray would look like as it exited the central channel. It most likely would not result is an even spray. Therefore, since all three pintles had too many negative traits, they were discarded as a plausible final solution. To design an injector which would rely on as few injection sites as possible, the swirl injector was investigated as the final design. The next section discusses the design process of the swirl injector.

2.2 Swirl Injector Design

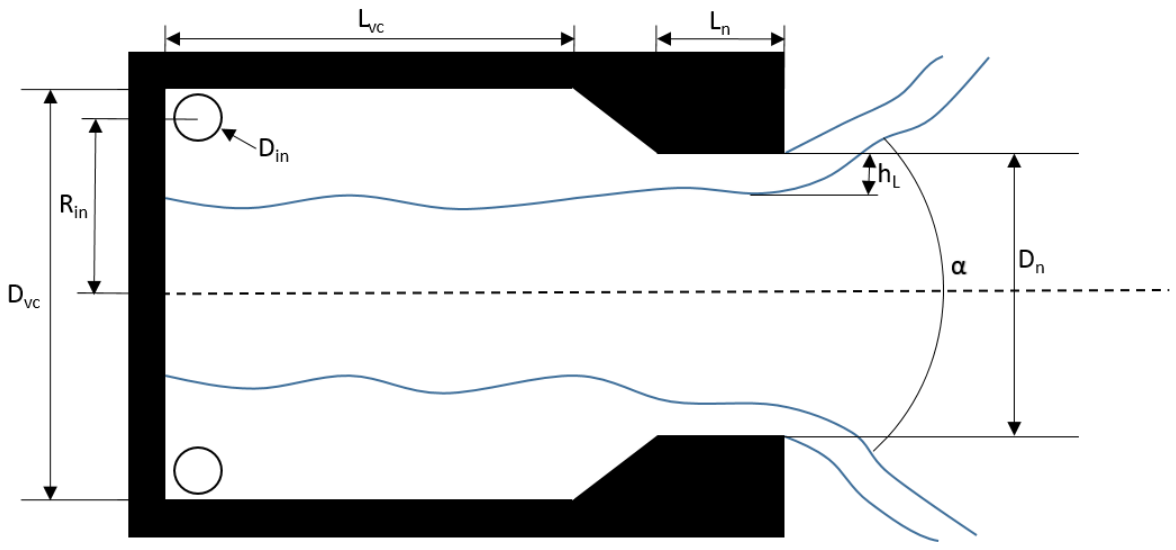

Figure 2.7 Swirl Injector Diagram

Figure 2.7 shows a diagram of a general swirl injector along with dimension that will be covered later in the section. The coaxial injector had the benefit of only needing one channel for the lead.

This allowed the channel to be large enough to not impede the flow of lead. The swirl injector was investigated as it only requires 1-4 injection sites to provide atomization. Using the same parameters of the above calculations along with only needing 2 inlets to a swirl injector, the following inlets areas were determined. Since the total flow area would remain the same with a similar discharge coefficient, using Equation 2.2 with 2 inlets yields an inlet diameter of 0.166 in. This is a much more favorable inlet diameter than the 0.035 in pintle inlet diameter.

To design the swirl injector, Dr. Vladimir Bazarov's previous work on swirl injectors was used [1]. The following equations are taken from his paper on injection methods for combustion stability.

$$V = \sqrt{\frac{2\Delta p}{\rho}} \tag{2.5}$$

Where V is velocity of the fuel, p is head pressure, and ρ is density. Once V, velocity, is solved it is plugged into Equation 2.6.

$$A_j = \frac{\dot{m}}{\rho V} \tag{2.6}$$

A_j is the ideal flow area required for a jet injector with flowrate of lead $\dot{m}$. Next the desired spray angle α is used to determine the non-dimensional parameter a. The spray angle refers to the angle of the spray cone exiting the swirl injector.

$$a = \frac{\tan(\alpha/2)}{1+\tan(\alpha/2)} \tag{2.7}$$

The non-dimensional parameter a is used to relate the discharge coefficient and φ, where φ is the ratio of the area of the swirl injector nozzle that is filled with liquid to the total area of the nozzle.

$$\sqrt{a} = \frac{(1-\varphi)\sqrt{2}}{\sqrt{2-\varphi}} \tag{2.8}$$

Another relation is provided to solve for the discharge coefficient of the injector.

$$\frac{\sqrt{a}}{C_d} = \frac{(1-\varphi)\sqrt{2}}{\varphi\sqrt{\varphi}} \tag{2.9}$$

Once the discharge coefficient is known, the flow area for the nozzle can be solved for using Equation 2.10.

$$A_n = \frac{A_j}{C_d} \tag{2.10}$$

In Equation 2.10, A_n refers to the nozzle area. Once we have the nozzle area, φ can be used to solve for the film thickness at the nozzle exit.

$$\bar{h}_L = 1 - \sqrt{1-\varphi} \tag{2.11}$$

In Equation 2.11 $\bar{h}_L$ is a non-dimensionalized version of the film thickness at the nozzle exit. Using the nozzle radius, the actual film thickness can be solved for using Equation 2.12.

$$h_L = \bar{h}_L * R_n \tag{2.12}$$

Where R_n is the radius of the nozzle solved from the area A_n. Next the location of the tangential inlets is determined. A radial location from the axis of the injector is used to place the inlets. The number on inlets usually ranges from 2 to 4. For this injector, 2 tangential inlets were chosen as the fewer inlets there are, the larger their dimeters need to be. Since lead has trouble flowing though small channels, the larger the inlets, the better the performance of the injector is likely to be.

First, a non-dimensionalized version of the radial inlet location is defined as $\bar{R}_{in}$. This variable is chosen and falls in between 1 and 3. For this injector 1.5 is chosen as it performs best in empirical studies [1]. To find the actual radial location of the inlets, the non-dimensional parameter is multiplied by the nozzle radius in Equation 2.13.

$$R_{in} = \bar{R}_{in} * R_n \tag{2.13}$$

With the location determined, the diameter of the inlets can be solved for using the following equations.

$$A = \frac{(1-\varphi)\sqrt{2}}{\varphi\sqrt{\varphi}} \tag{2.14}$$

$$D_{in} = \sqrt{\frac{4A_n\bar{R}_{in}}{An\pi}} \tag{2.15}$$

In Equations 2.13 and 2.15, R_{in} is the radial location of the inlets, which is not to be confused with D_{in} which is the diameter of those inlets. A in Equation 2.14 is an injector geometrical characteristic. Since the inlets are now dimensioned, the vortex chamber, or main body of the injector, must be sized. Equations 2.16 and 2.17 calculate the diameter and the length of the vortex chamber respectively.

$$D_{vc} = 2R_{in} + D_{in} + \delta_t \tag{2.16}$$

$$L_{vc} = 2.5D_{in} \tag{2.17}$$

δ_t is a mechanical margin for wall error that is equal to 0.008 inches. The final dimension needed is the length of the nozzle which Bazarov states should be between 0.04 and 0.06 inches [1]. Figure 2.7 shows a diagram of a swirl injector with the above dimensions labelled.

The first swirl injector tested was designed using this procedure. In order to test the design, a CAD model of the injector was created and was 3D printed using PLA plastic material on a Lulzbot Mini printer. The injectors took between 8 and 30 hours to print based on the size of the injector being printed and whether or not it had an air manifold. Since the injectors were only being tested with water flows, there was no need to fabricate an injector that could withstand molten lead. Figure 2.8 shows a CAD drawing of the injector tested. The teardrop shape of the inlet is due to the front facing cross section. The channel is circular as seen in the top view cross section.

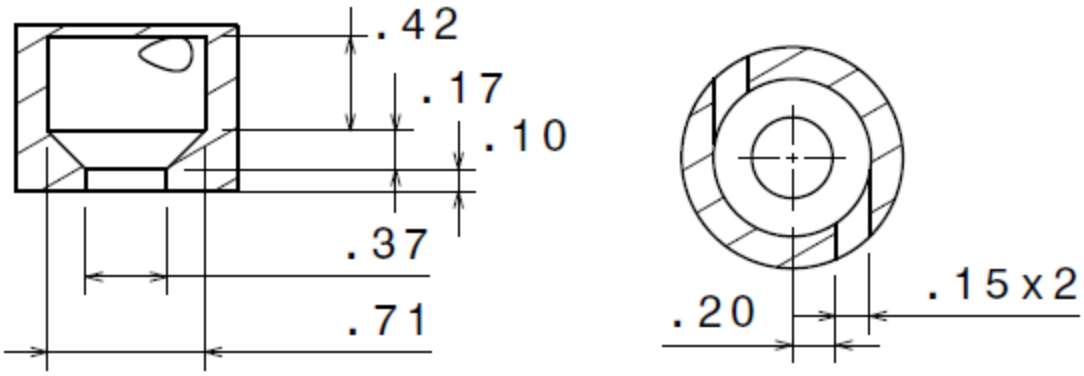

Figure 2.8 First Swirl Injector Designed. Dimensions in Inches

This injector was designed under the desired operating conditions of 6000 lbs of lead per hour. One discrepancy from the above equations is the length of the nozzle. Bazarov states that the nozzle should be 0.04 to 0.06 inches in length [1]; however, to make it easier to 3D print, that length was increased to 0.1 inches. In order to test with water, parameters had to be adjusted so the resulting spray would be similar to that of a lead spray. For pure liquid testing without any air impingement to simulate the oxidizer, the only parameter that has to be matched is volumetric flowrate in order to simulate a similar flow. In order to accomplish this, the velocity of water is set equal to the desired velocity of lead. Equation 2.5 then is used to determine the amount of pressure is needed to achieve the same velocity with water.

2.3 Swirl Injector Testing

The test stand setup was a very simple configuration. The injector testing was done with water and air at less than 50 psi. This allowed every test article to be 3D printed. Printing allowed for rapid design and prototyping. The test article was set up on a stand made of Unistrut show in Figure 2.15. Water was brought in from a 40 psi line and air was brought in from a 100 psi line. The water

fed into a manifold that surrounded the swirl injector and entered through the tangential inlets. Air entered on opposite sides of a manifold then through a ring to impinge on the water spray. Figure 2.9 shows the test stand setup.

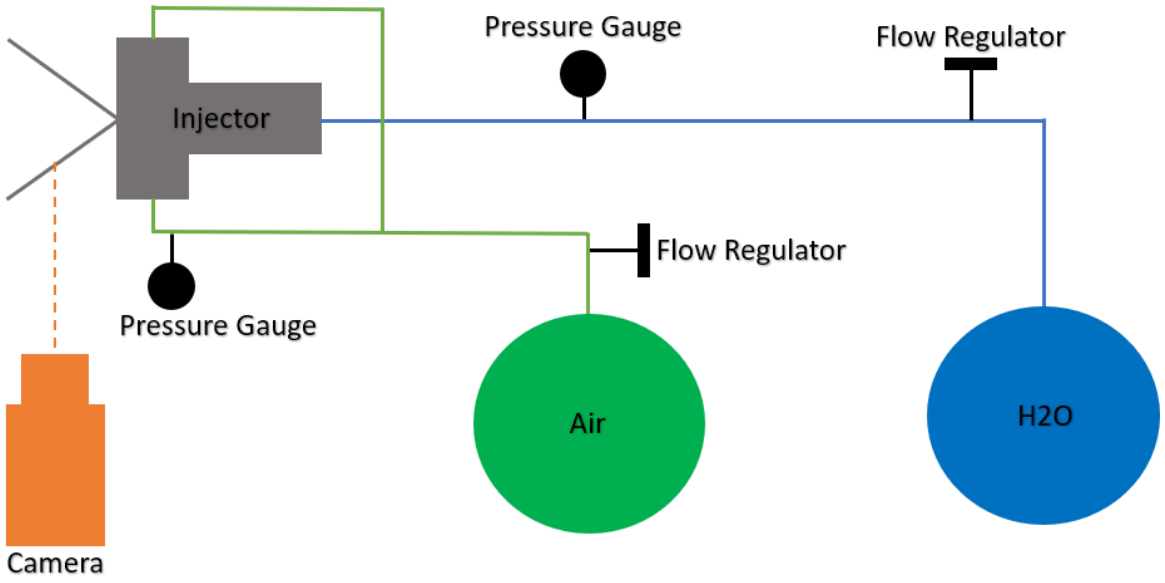

Figure 2.9 Injector Test Setup

The camera used in the experiment was a Phantom vSeries high speed camera capable of up to 4000 frames a second. This would allow for a better understanding of what the spray was doing and a closer look at where the sheet was breaking up. Figure 2.10 shows the development of the spray from the above swirl injector design. This design will be referred to as Mk. 1. Table 2.1 lists all of the injectors and their numbers respectively.

Table 2.1 Injector Designs

Injector	Design Method	Small Air Ring	Med. Air Ring	Large Air Ring	Cone
Mk. 1	Bazarov	no	no	no	no
Mk. 2	Optimized	no	no	no	no
Mk. 3	Bazarov	no	no	yes	no
Mk. 4	Optimized	no	no	yes	no
Mk. 5	Optimized	yes	no	no	yes
Mk. 6	Optimized	yes	no	yes	yes
Mk. 7	Optimized	no	yes	no	yes

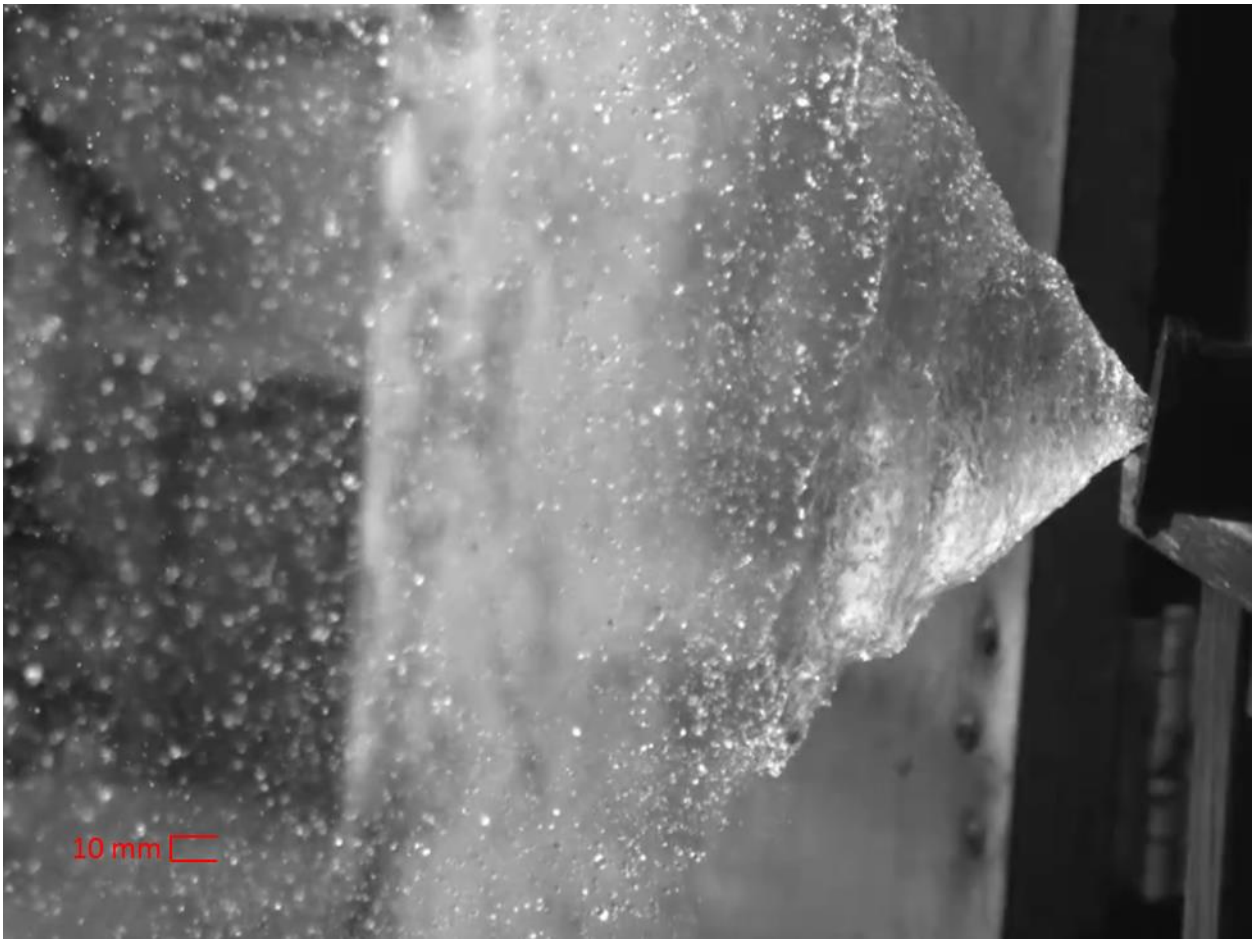

Figure 2.10 Spray Resulting From the Swirl Injector Test of Mk. 1

From the high speed video, the distance it takes for the spray to break up can be measured. Using a reference distance in the video, the camera software can also give an estimate for the droplet size, although it is just used as an estimate. For the first few tests, only water was used without air

impingement to ensure that the design of the swirl injector was sound and the 3D printed part functioned as intended.

An interesting phenomena seen in the videos is the instability waves in the cone just before breakup. They appear to contain the same frequency as the rotational frequency of the spray. This leads me to believe that changing the interior of the swirl injector could change how the breakup of the cone functions. To observe the impact of changing the interiors of swirl injectors, ratios were used from a paper on optimizing swirl injectors. It had SMD droplet size averages for multiple different ratios of vortex chamber length to vortex chamber diameter and nozzle length to nozzle diameter.

The paper showed results of the smallest SMD of the droplets for a nozzle length to diameter ratio of 1.44 and a chamber length to diameter ratio of 1.25 [4]. The original injector designed with Bazarov's equations was modified by keeping the diameters of the nozzle and swirl chamber constant and extending the lengths of each component until the previously stated ratios were reached. The injector was also 3D printed and tested. Figure 2.11 shows the resulting spray from this "optimized" injector Mk. 2.

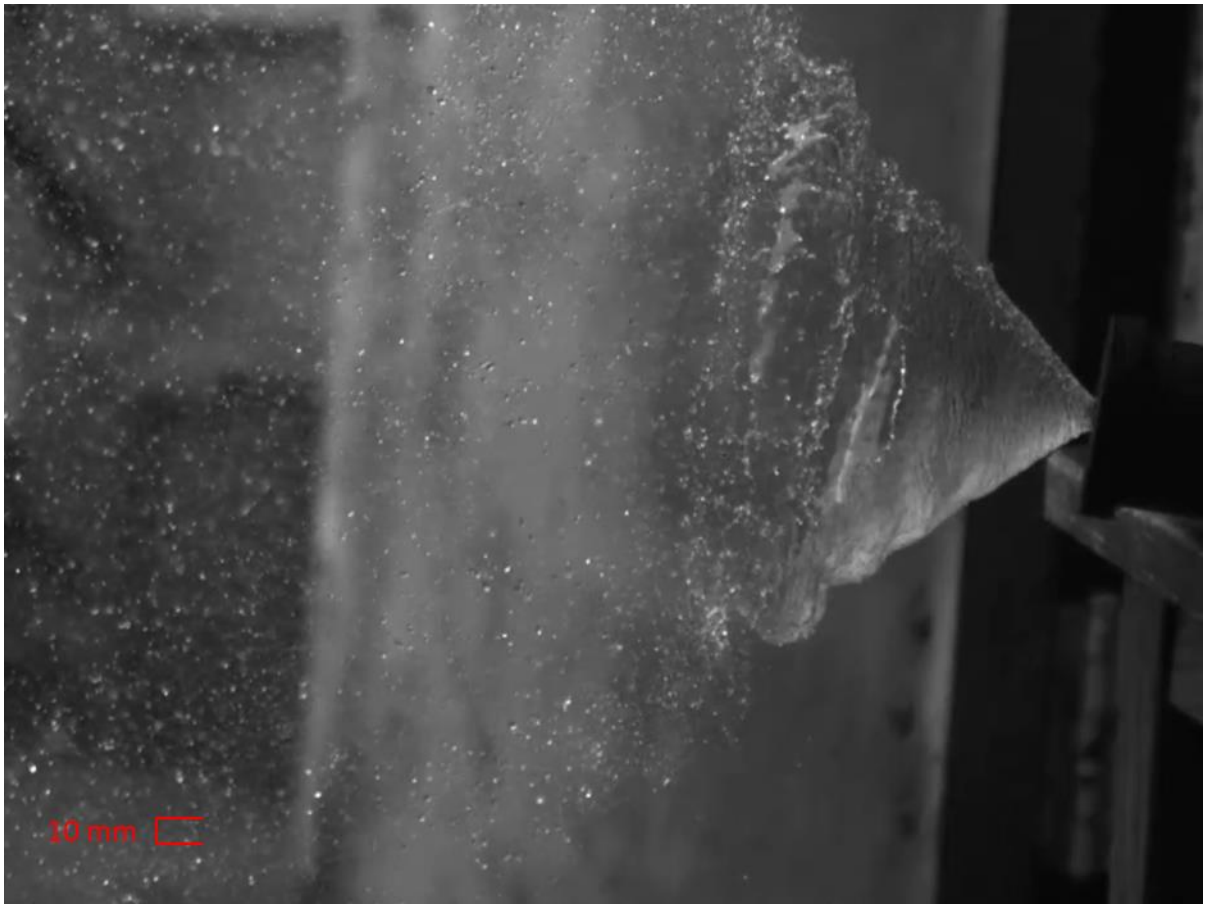

Figure 2.11 Spray Test of Optimized Injector Mk. 2

After using the camera software to get approximate droplet sizes, the results showed that these optimized ratios resulted in smaller final droplet size. It also increased the size of the instability waves at the edges of the spray cone. Increasing the size of the waves increased how vigorously the sheet breaks up leading to smaller droplet sizes. This shows that to reduce droplet size, increase the size of the instability waves. Due to the smaller droplet sizes associated with the optimized ratios, they are used in most of the following swirl injector designs.

After the water tests were completed, an injector with the optimized dimensions (Mk. 2) was fabricated out of stainless steel for lead testing. The lead testing setup resembled the water testing

setup with a few differences. Lead flowed through the top of the injector into a manifold that surrounded the injector. This served 2 purposes: to feed the tangential inlets of the injector and too keep the inject warm enough to prevent the lead from freezing on the inside of the swirl chamber. The first tests run also did not make use of air. The first tests were done to see if the lead would be able to flow through such small channels into a swirl injector and to function in a similar way to the water. The same high speed camera was used to film the lead flow.

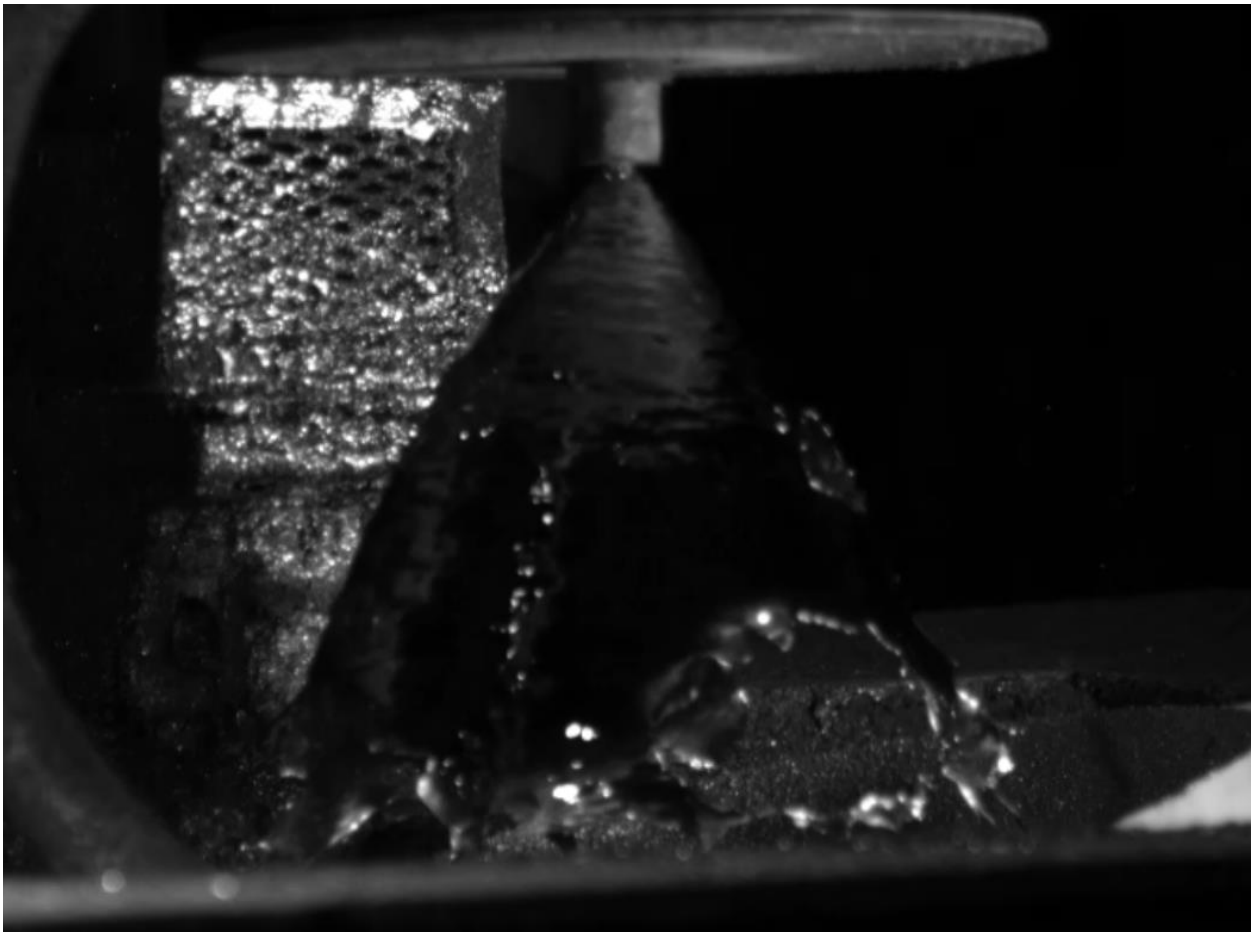

Figure 2.12 Lead Flow from Injector Mk. 2 at 45 Hz

Figure 2.12 shows the first run of the lead flow through the injector. The pump that pushed lead through the injector only had output in Hz so the actual head pressure of the lead is unknown. Trying to measure mass flow rate and back calculate for pressure led to wide variation through a

few trials and more data was unavailable. It is predicted that the lead pressure was between 40 and 60 psi.

Lead's surface tension is six times greater than water. This leads to the sheet of lead holding together for a much longer distance before breaking up as seen in Figure 2.12. The breakup at this pressure is also much different from water. When the lead is finally stretched too thin, it breaks off in sheets and ligaments instead of droplets. In order to try and get the breakup to more resemble droplet the pump was increased to 60 Hz. This is likely in the 60 to 90 psi range. Figure 2.13 shows the results from this test.

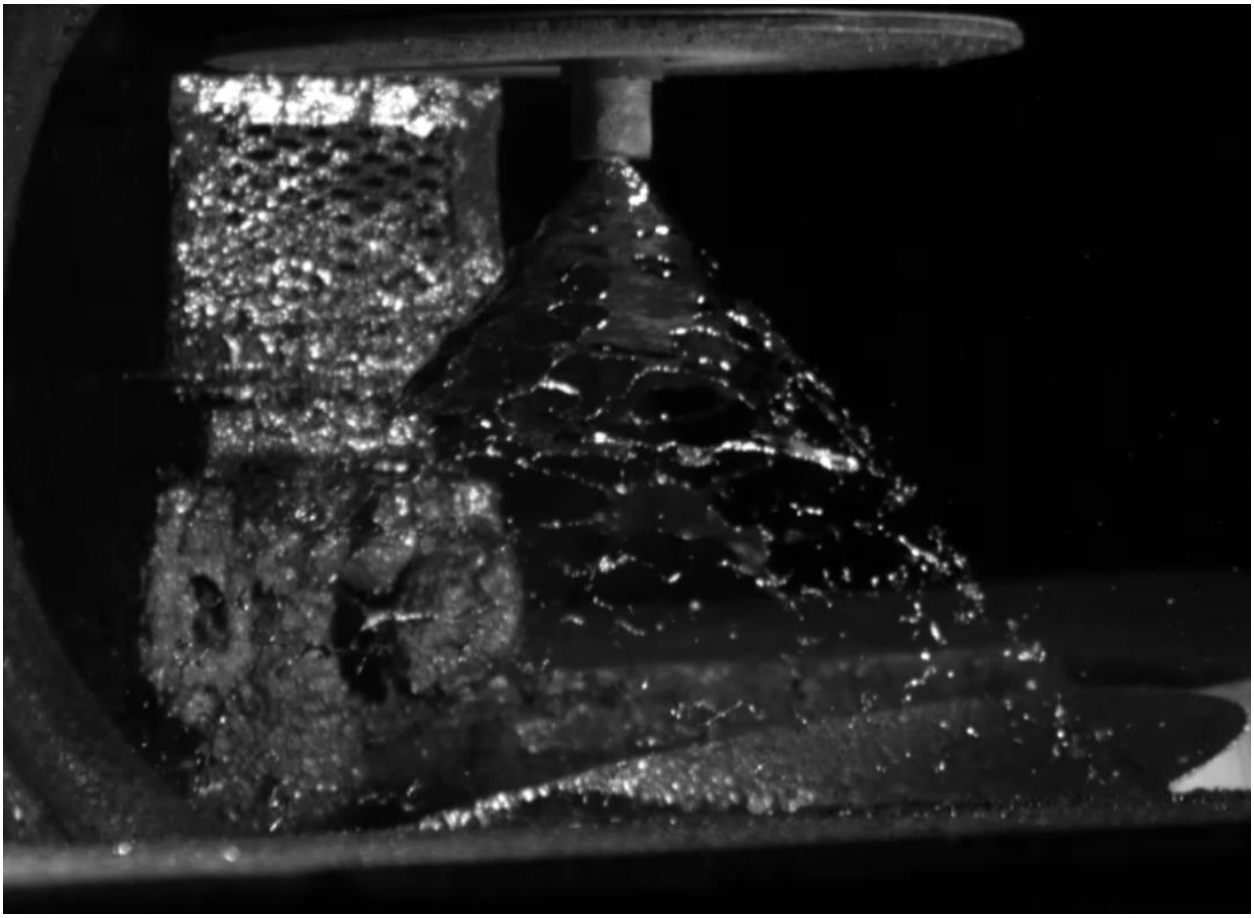

Figure 2.13 Lead Flow from Injector Mk. 2 at 60 Hz

At higher pressures the lead did start to breakup into a combination of droplets and ligaments. While droplets would be the ideal form of breakup for atomization and combustion, the ligaments can be assumed to break up further once an atomizing oxidizer is introduced to the flow. This test was successful as it proved lead will flow through the inlet channels and can be atomized to some degree with a swirl injector. The next step is to add air to the injector.

2.4 Airblast Atomization Design and Testing

The current method of adding air to the Barton pot is to bring it in axially along the blade rotor. An improvement to the system would be to bring the air in with the lead through the injector. This would provide the injector a source of secondary atomization along with allowing the oxidation process to begin immediately thus reducing the residence time inside the Barton pot. The rest of the chapter is dedicated to the design process and iterations of the oxidizer portion of the injector.

The first design was a simple air ring around the injection site that was fed by a manifold that surrounded the injector. It was fed by a line on each side of the manifold to help ensure a more constant flow of air. Mk. 3 and Mk. 4 were the same style on injector, but Mk. 3 used Bazarov's design method while Mk. 4 used the optimized ratios. Figure 2.14 shows a CAD drawing of the injector Mk. 4.

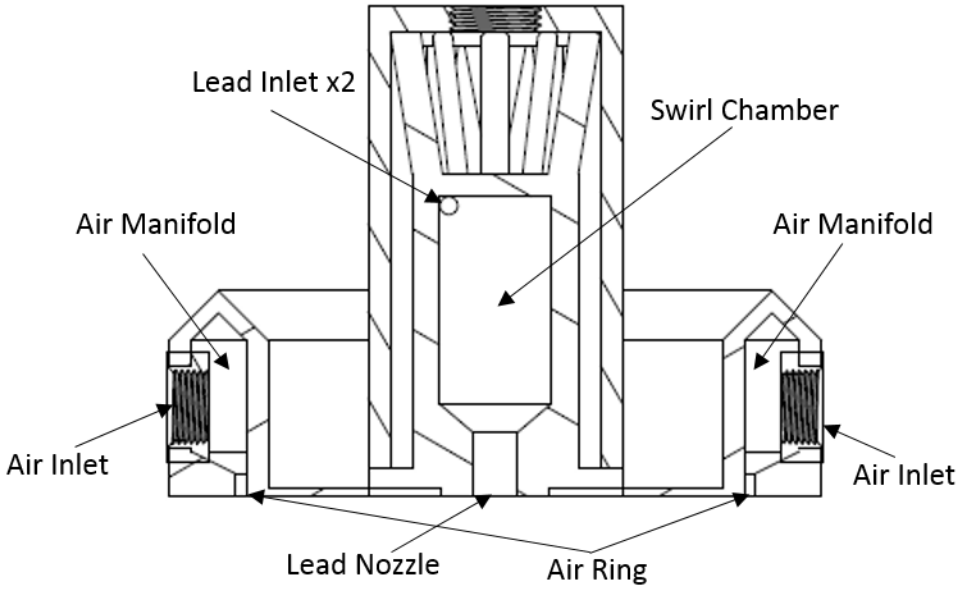

Figure 2.14 Swirl Injector with Attached Air Manifold Mk. 4

The design of the Mk. 4 injector and air manifold was influenced by the need to be able to 3D print the design. Having a triangular top to the air manifold and supports holding the water manifold above the injector provide no benefit to the performance of the injector. Those features are purely there for the ease of 3D printing the injector. Figure 2.15 shows the injector mounted on the test stand and Figure 2.16 shows the spray resulting from the injector with the oxidizer ring.

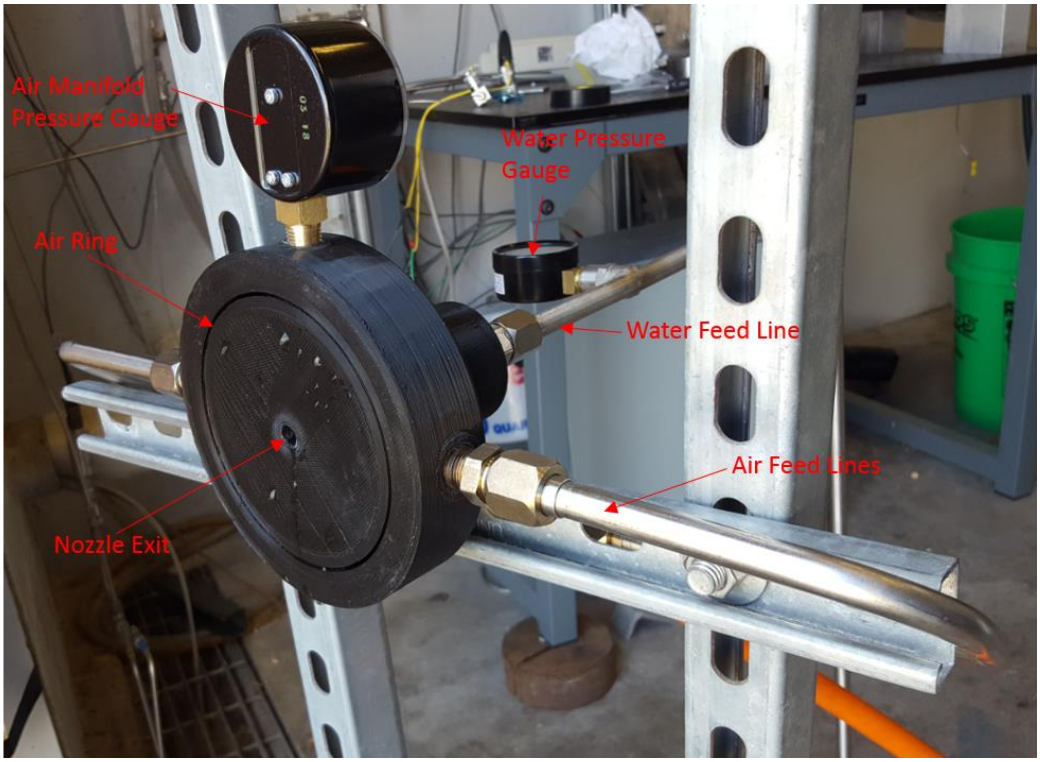

Figure 2.15 Injector Mk. 4 Mounted on the Test Stand

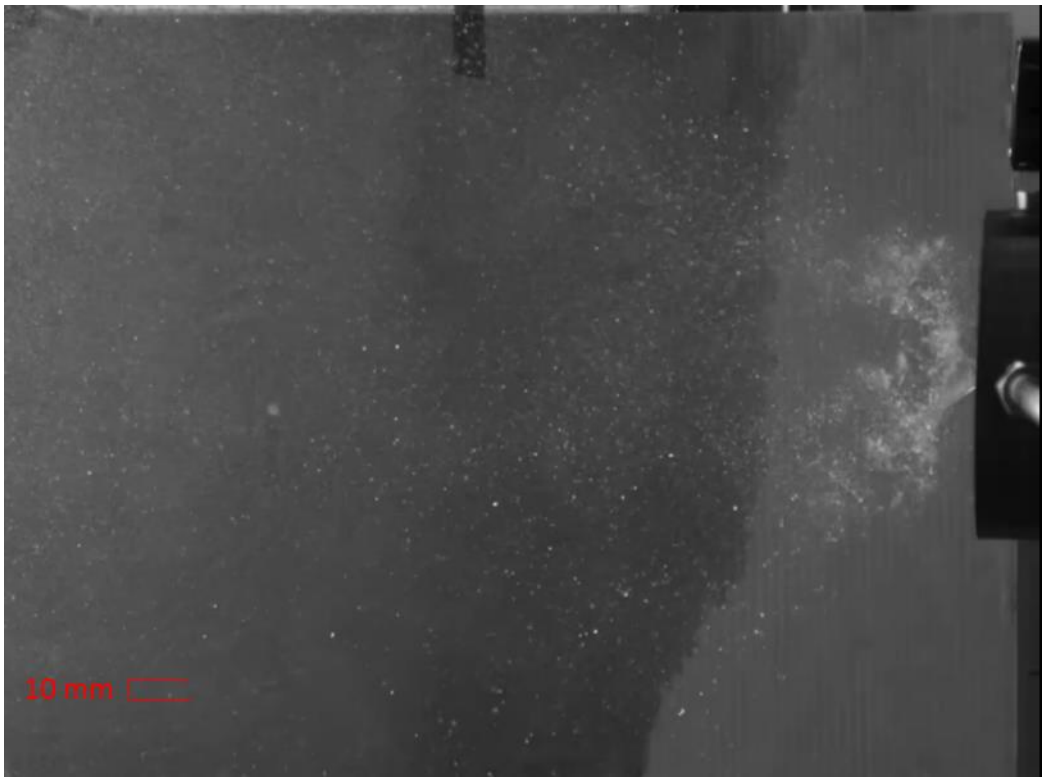

Figure 2.16 Spray from First Test of Injector with Air Ring Mk. 4

As seen above in Figure 2.16, the spray is finely atomized into droplets. Based on the estimated droplet size values from the camera software, these droplets fall in the 10-100 micron range. When using this system to spray lead and air into a Barton pot, the resulting atomization along with the Barton pot's own atomization was expected to produce powdered lead oxide that was already in size specification without the need for milling. Moving forward, the injector and accompanying air manifold was fabricated out of stainless steel for lead testing.

The lead testing was run on a stand that just fed into a collection bin in order to be observed. If the injector had been sprayed directly into a Barton pot, the results could not have been seen or recorded other than simply observing the resulting particle size. The testing revealed that the lead was freezing immediately after exiting the injector. This lead to massive lead accumulation on the injector face and shutdown of the lead flow.

After reviewing what had happened, Figure 2.16 helps to explain how the lead froze. As seen above, the force of the air exiting the injection ring caused a low vacuum force to be applied to the spraying water. This force pulled some of the water droplets back against the injector faceplate. For the water testing this didn't cause a problem in creating an atomized spray. However, during the lead testing the same phenomenon occurred. Except when the lead hit the faceplate, it froze on contact. With the amount of droplets that came in contact with the faceplate, lead piled up very quickly on the face of the injector eventually sealing off the inlet. The rest of the chapter is dedicated to the design process of keeping the lead off of the faceplate when using an air ring.

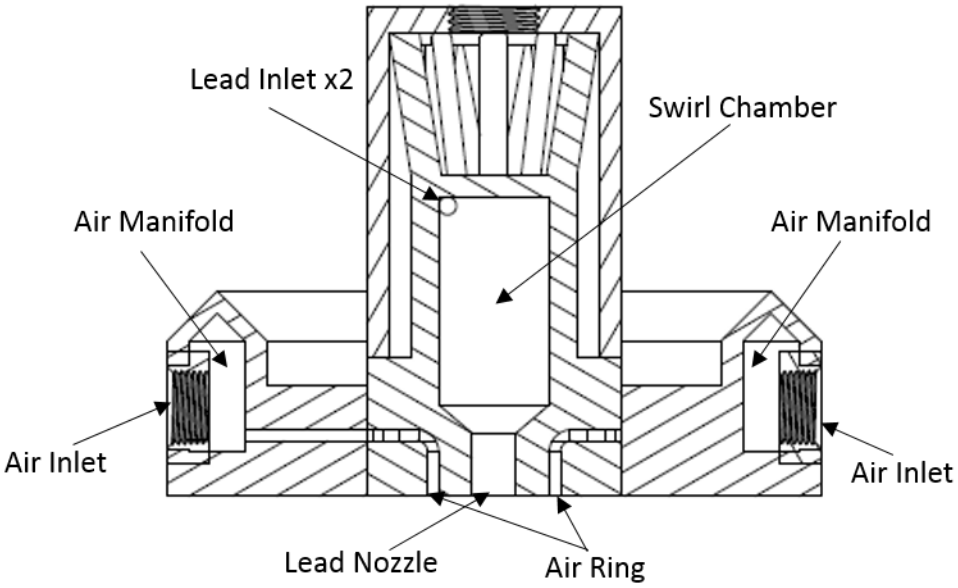

Figure 2.17 Next Iteration of the Injector Mk. 5

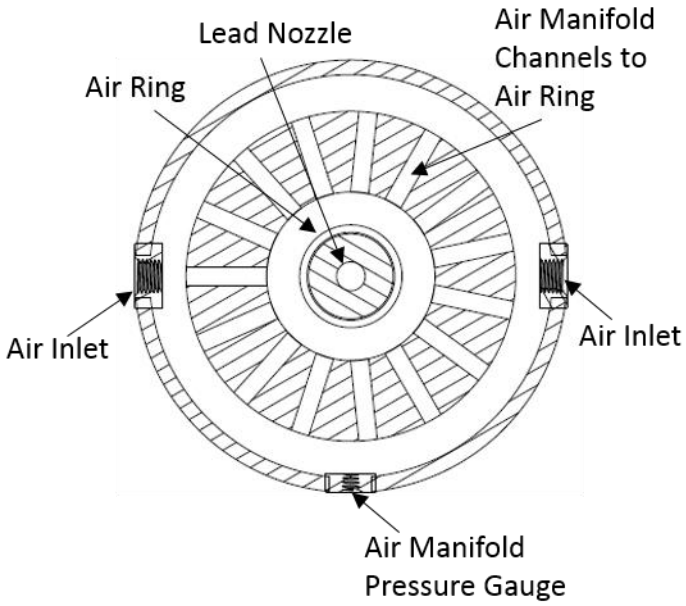

Figure 2.18 Section View Cut at Air Manifold of Mk. 5

Figures 2.17 and 2.18 show the next design of the Mk. 5 injector. The air atomization ring was moved very close to the nozzle exit. This would reduce the amount of the injector face that was

susceptible to getting splashed with droplets. Ideally the ring would have been fed circumferentially from the manifold. However, to 3D print the design, the inner ring had to be fed through a ring of channels instead. That is why, in Figure 2.17, the right side of the inner ring does not appear to be connected to the air manifold. This is simply because the channels are not symmetric and this cross section only shows one on the left side of the injector. Figure 2.18 is a cross section of the channels that feed the air ring to better illustrate Figure 2.17. Figure 2.19 shows the spray testing results from the Mk. 5 injector design.

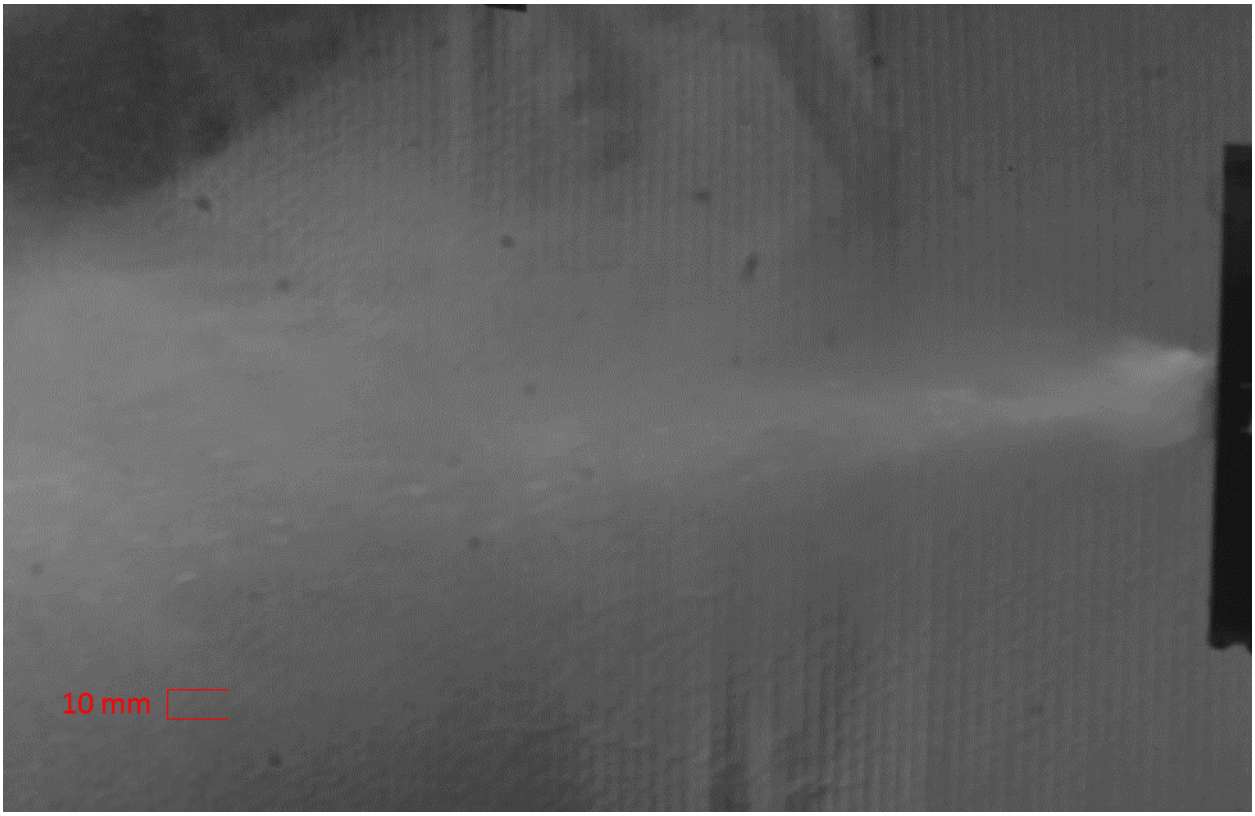

Figure 2.19 Spray Test Result from Mk. 5 Injector

The injector produced a well atomized spray, but in Figure 2.19, it is clear that the center of the spray is denser, thus made up of larger droplets. This uneven distribution of droplet sizes would still require milling after injection if those large drops did not break up enough. The small area of the faceplate in between the water nozzle exit and air ring was not able to keep completely clear

of water. If lead can splash against this small area it has a chance to freeze. A chance that the lead could freeze somewhere generally means that it will, so a slight modification of this injector was tested. A small cone was put on the end of the injector nozzle shown in Figures 2.20, 2.21, and 2.22. This cone filled the space between the ring of air and the nozzle exit. Figure 2.20 shows the results of the test.

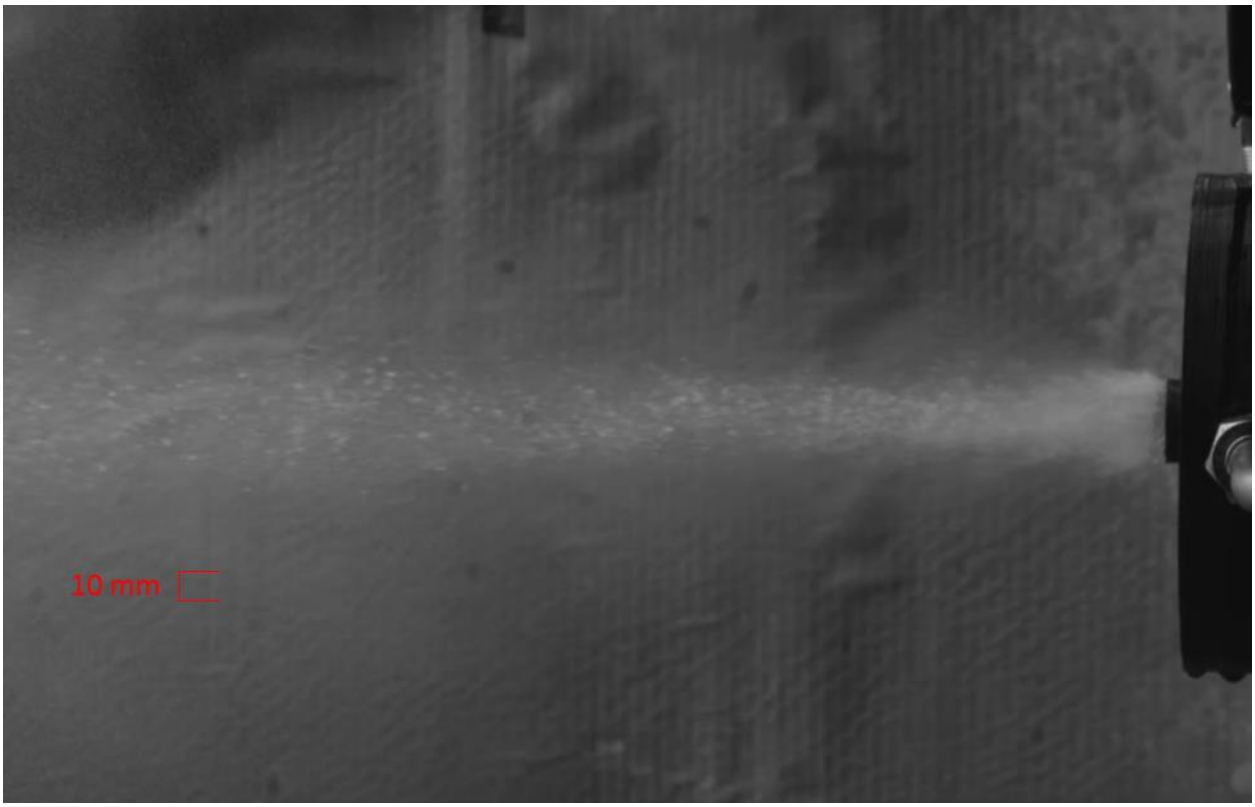

Figure 2.20 Spray Test with Small Air Ring and a Nozzle Cone Mk. 5

Adding the cone to the end of the nozzle created a more successful test. The droplets in the center of the spray are still significantly larger than the rest of the spray. However, the nozzle kept the water completely off of the injector face. With this setup spraying into a Barton pot it is unlikely that the lead would freeze during injection. If the atomization methods in the Barton pot, such as the spinning blade and baffle plate, could ensure secondary atomization of the larger droplets, this configuration could work as an injection system. The spray is atomized and kept in a fairly tight

cone to prevent lead from hitting the walls. Although a successful test was completed, the design was altered again in order to create an injector which could hit atomization targets without secondary breakup.

Designing the Mk. 6 injector employed aspects from both of the previous injectors. The inner ring is a necessity, but it causes the spray to be too centralized and group into larger droplets. Therefore, the next design utilized a large and small air ring. The cone was kept on the end of the nozzle in order to help prevent water from getting on the injector faceplate. An addition to the next injector was an opening on the faceplate in between the two rings. This opening led back to a vacuum gauge to measure the strength of the vacuum that was pulled by the force of the air. Figures 2.21, 2.22 and 2.23 show drawings of the new injector and a spray test respectively.

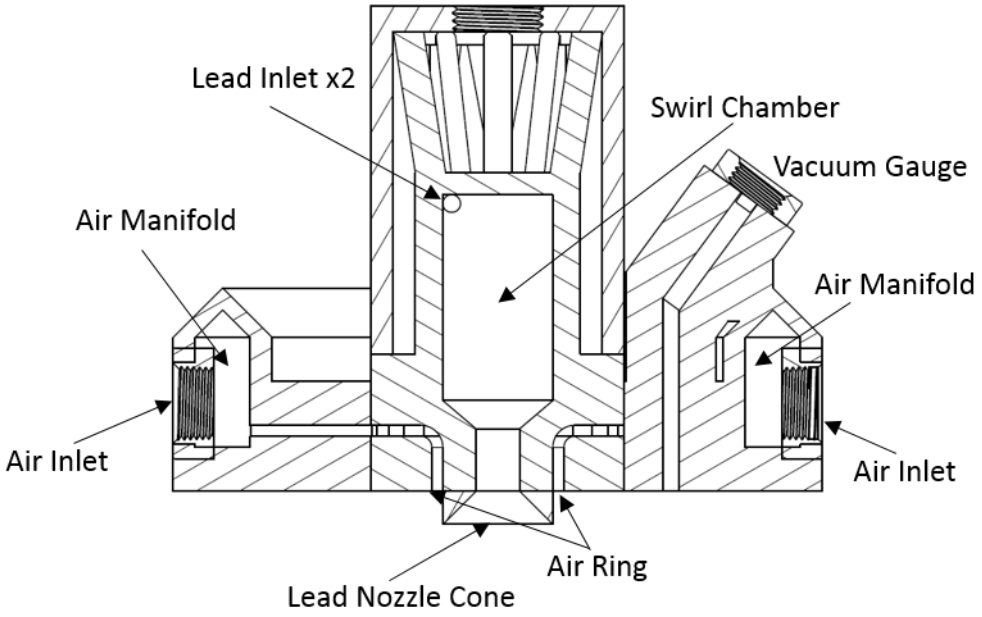

Figure 2.21 Cross Section of Mk. 6

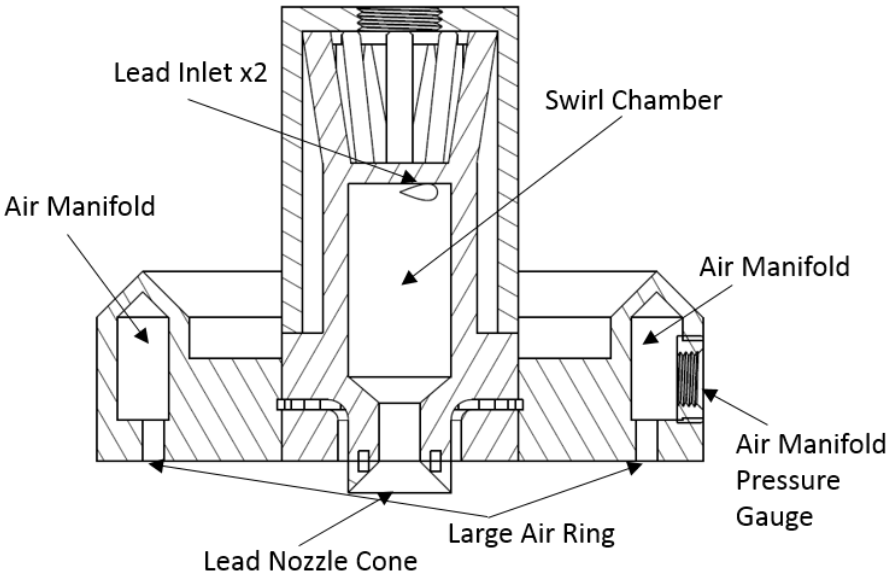

Figure 2.22 Mk. 6 Cross Section Rotated 90 Degrees

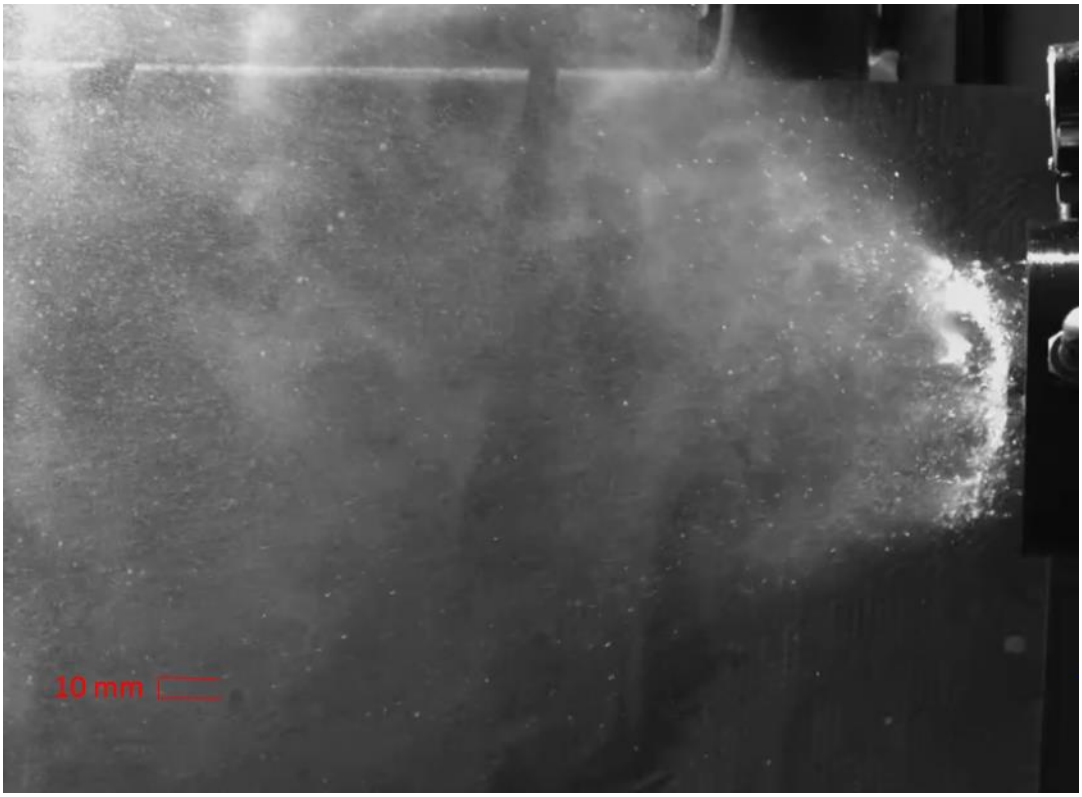

Figure 2.23 Spray Test of Double Ring Injector Mk. 6

When testing the double ring injector it was determined that the vacuum strength was between -1 and -2 mmHg. Figure 2.23 shows that this is more than enough to pull the water droplets back against the faceplate of the injector. If this setup was tried with lead it would result in the same freezing even with the cone and inner ring. It is possible that this configuration could work if the inner and outer ring pressures could be controlled separately. However, introducing that much complexity to the injector was not desired.

To reach the final design, all of the previous injectors were evaluated based on the positive and negative characteristics. The cone attached to the end of the nozzle was beneficial in every case tested. It would be beneficial in the final design. The only cases that resulted in no water on the faceplate were the designs that had the air flow around the cone and no other airflow. Since the design that just had the cone and the small ring didn't work optimally, the cone was enlarged. This allowed for the air ring to be enlarged as well without ending up with open faceplate area. To determine how large to make the cone, the tests with the small cone and single are ring were used. First the angle the spray was coming off the cone was measured. That angle was then applied at the point where the droplets had met in the middle of the spray. A line was traced back to the faceplate of the injector and the cone was sized and printed. Figure 2.24 shows the results of the Mk. 7 test.

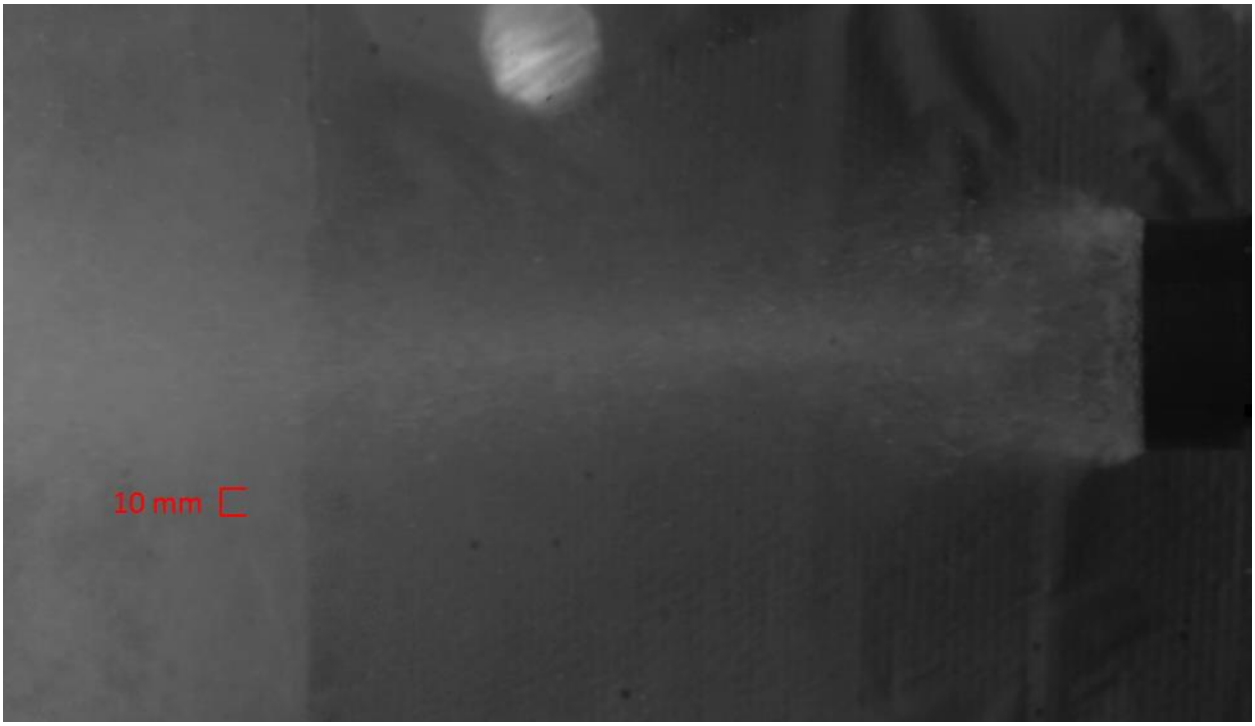

Figure 2.24 Final Spray Test with the Large Cone Mk. 7

As seen in Figure 2.24 above, the water coming off of the cone atomizes perfectly with no central droplets coalescing into larger droplets. The resulting spray has small droplets and an even distribution of sizes. Due to these results, this is the recommended configuration for lead atomization. One possible point of failure could be the air cooling the nozzle enough for the lead to freeze while running along the surface of the nozzle. When installed inside of a Barton pot this is unlikely though due to the high temperatures experienced inside the system. Mk. 7 is the final injector design tested.

2.5 Chapter 2 References

[1] Bazarov, V. “Design of Injectors for Self-Sustaining of Combustion Chambers Acoustic Stability.” *Moscow Aviation Institute.* 2006. 10.2514/6.2006-4722.

[2] Dudaney, R., Heister, S. “Design and Fabrication of Novel Lead Oxide Combustion Injector.” April, 2017.

[3] Heister, S. “Pintle Injectors.” *Handbook of Atomization and Sprays*, Springer, 2016, pp. 647–656.

[4] Rashad, M., Yong, H. “Experimental Investigation of Variation in Radial Values of SMD and Mass Flux with Change in Geometric Ratios in Pressure Swirl Atomizers.” *Beihang University, Beijing.* 2017.

CHAPTER 3. LEAD COMBUSTION AND ADVANCED CHAMBER DESIGN

Much less is known about lead combustion than other metal fuels that have been studied for propulsion applications. This serves as a substantial impediment to design of advanced combustion devices and served as a motivation for a fundamental analysis to identify the rate controlling mechanism. Time scales are identified for chemical kinetic and diffusion processes in Sections 3.1 and 3.2 of this chapter in order to shed light on the controlling mechanism. A basic energy balance is developed to determine the relationship between injected water flow and combustion temperature. Results from these studies then inform the design of an advanced lead combustor in Section 3.4. Here the intent is to explore the design space to illustrate and contrast reactor footprint when compared to existing Barton reactors. The chapter concludes with Section 3.5 that presents parametric studies detailing the design of the advanced combustor over a range of operating conditions.

3.1 Kinetic Oxidation Rates

While improving the Barton pot is the immediate purpose of this research, the end goal is to create a system that produces lead oxide more effectively than the Barton pot system. It is believed that a simple rocket-style combustion chamber with lead and air injection could serve this purpose. To design such an injector, more needs to be known about the chemical properties of combustion for lead and lead oxide. This chapter will discuss whether the oxidation reaction of lead is kinetically controlled or diffusion controlled, how that was discovered, and the effect that it has on a combustor design.

Not much data exists on the combustion rate of lead. The only data found is in a paper on oxidation kinetics of lead [8]. Lead oxidation is a surface reaction, and as such, the surface area of the lead plays a large role in the rate of oxidation. Oxidation data from literature was measured in change in weight of the lead with respect to the amount of surface area of the lead. The change in weight measured corresponds to the amount of oxygen that bonded to the lead atoms. The following figure is the results of the empirical oxidation work.

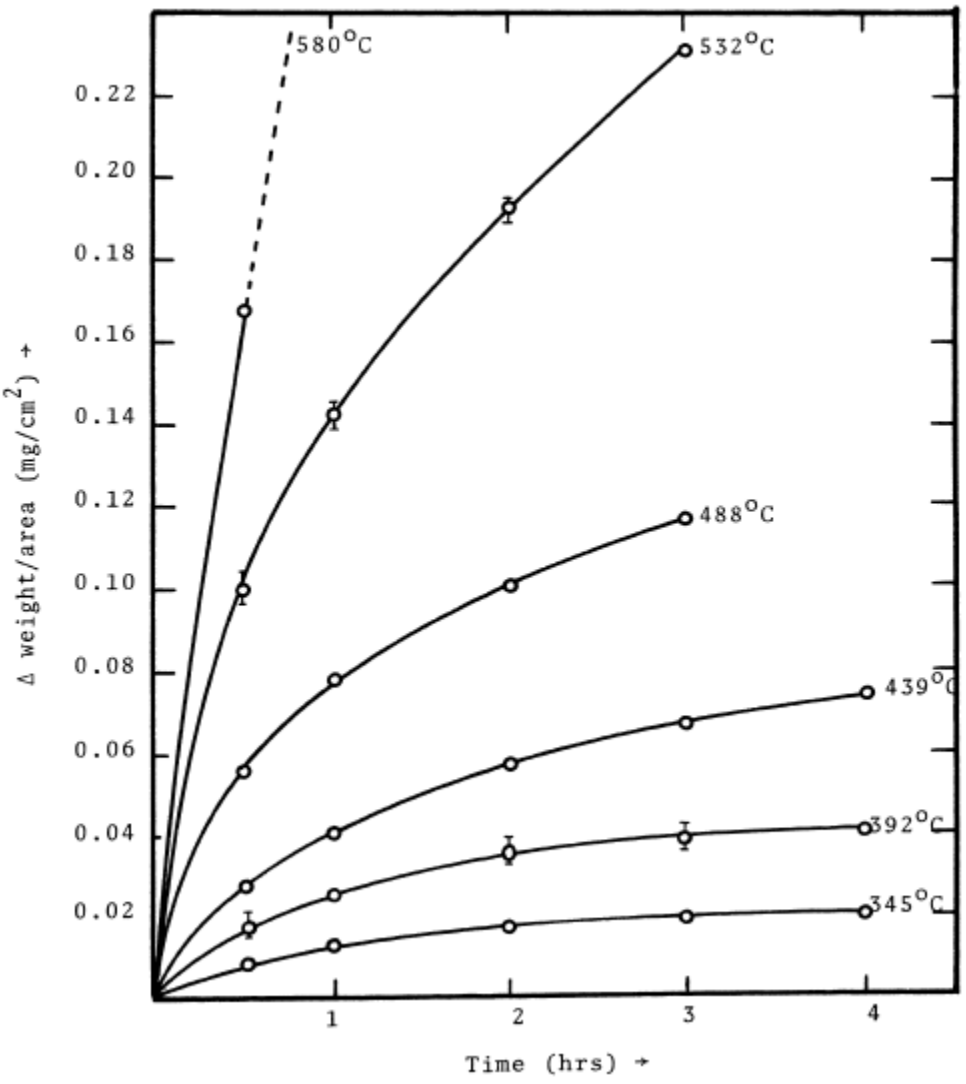

Figure 3.1 Lead Oxidation Results [8]

This data is hard to use for a combustor due to a few reasons. First, it only contains results for temperatures up to 580 C, 853 K. As shown on the x-axis, the oxidation times are in hours. The lead is fully oxidized once each curve levels out. The data above is formed from a flat surface of lead as well. Since the lead in a combustor would be in droplet form, the mass to surface area ratio would be a lot lower than the flat surface of lead that determined the rates in Figure 3.1 [8]. To determine the rates, the adiabatic flame temperature of lead oxidation was found through the following steps.

$$Pb + \frac{1}{2}(O_2 + 3.76N_2) \rightarrow PbO + 1.88N_2 \tag{3.1}$$

Using the chemical formula in Equation 3.1, an enthalpy balance was set up.

$$\left(\bar{h}_f^o + \Delta h\right)_{Pb,r} + \frac{1}{2}\left(\bar{h}_f^o + \Delta h\right)_{O_2,r} + 1.88\left(\bar{h}_f^o + \Delta h\right)_{N_2,r} =$$

$$\left(\bar{h}_f^o + \Delta h\right)_{PbO,p} + 1.88\left(\bar{h}_f^o + \Delta h\right)_{N_2,p} \tag{3.2}$$

All of the heat of formation data ($\bar{h}_f^o$) as well as equations for enthalpy change of each chemical (Δh) was taken from the NIST website [2]. The adiabatic flame temperature of lead oxidation was calculated to be approximately 1900 K at stoichiometric conditions. For the oxidation process it is desired that the lead remain in a liquid state as gaseous lead is an extreme health hazard and would require an advanced facility. Since the boiling point of lead oxide is 1535 degrees C, the extrapolated values were extended up to 1300 C to guarantee the lead stays in a liquid state. In order to extrapolate the data, equations were found to fit the curves shown in Figure 3.1. The following table shows those curve fits.

Table 3.1 Oxidation Rate Curve-fit Equations

Temperature	Curve for Time (hours) vs Mass Change over Surface Area (mg/cm^2)
345 C	$\Delta M = -0.006t^2 + 0.017t$
392 C	$\Delta M = -0.016t^2 + 0.04t$
439 C	$\Delta M = -0.026t^2 + 0.065t$
488 C	$\Delta M = -0.06t^2 + 0.138t$
532 C	$\Delta M = -0.114t^2 + 0.255t$
580 C	$\Delta M = -0.168t^2 + 0.418t$

To extrapolate the burn time for a certain droplet, first the ratio of mass required to oxidize the droplet to surface area of the droplet is calculated. This is found by simply balancing Equation 3.1 to find the mass of oxygen required as the change in mass of the droplet shown in the following equations.

$$V = \frac{4}{3}\pi\left(\frac{D}{20000}\right)^2 \tag{3.3}$$

The droplet volume V is in mm^3 when D is the diameter in microns.

$$m_{Pb} = 10.65V \tag{3.4}$$

The droplet mass is found in mg when the volume is multiplied by the density.

$$m_{O_2} = 16 * \frac{1}{2} * \frac{m_{Pb}}{207{,}200} \tag{3.5}$$

The mass of oxygen is then found by dividing the mass of lead by its molecular weight and multiplying by moles of oxygen and molecular weight of oxygen. For example, a 10 micron radius droplet has a mass of oxygen required to surface area ratio of 0.0685 mg/cm^2. Plugging this number into the value for ΔM in the equations in Table 3.1 gives a burn time for each temperature. These data points are then used to create another curve-fit for burn time vs temperature. This line is plotted in Figure 3.2.

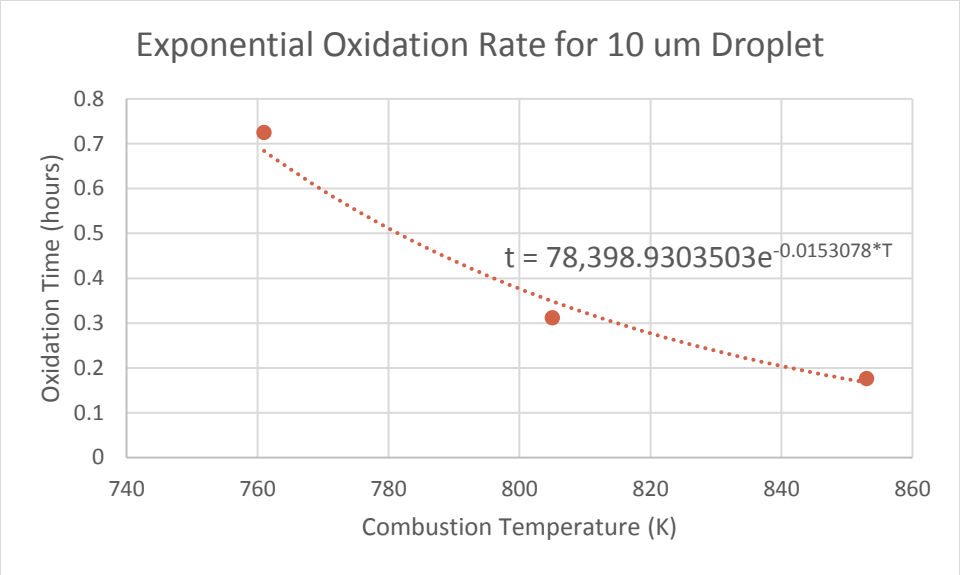

Figure 3.2 Exponential Oxidation Time vs Temperature

Only the three data points from 488 C (761 K), 532 C (805 K), and 580 C (853 K) were used because the other 3 temperatures were too low to oxidize the entire droplet in a reasonable amount of time. These three data points yield and equation specific for a 10 micron droplet.

These curve-fits give an extremely rough estimate for the kinetic oxidation times of droplets. These values are used as only a rough guideline as the empirical data is extrapolated to a large degree and error in actual accuracy is to be expected. For a 10 micron diameter droplet at 1300 C, it takes 10 milliseconds to oxidize. The maximum air speed the blowers for the injector can produce is approximately 300 ft/s. Operating at max air speed is desirable as it will produce the best atomization. If the droplets are moving at 300 ft/s, in 10 milliseconds the droplets will travel 3 ft. However, if the temperature is lowered just 50 degrees to 1250 C, it takes 21 milliseconds and requires a 6 ft long chamber. Lowering the temperature quickly causes the chamber to grow to lengths that are too long for a combustion chamber to be practically used. If the rough estimates

of kinetic rates are to be believed, the temperatures would need to exceed 1250 C in the chamber. However, since lead combustion is a surface reaction, kinetic rates may not dominate the burn time. Therefore, the oxidation rate according to diffusion rates is evaluated.

3.2 Diffusion Oxidation Rates

If the diffusion based combustion/ oxidation rate of lead is faster than the predicted kinetic rate, it can be determined that the oxidation rate is diffusion controlled. Yetter and Dryer wrote a paper describing the burn rates of metal droplets due to diffusion [9]. If the calculated diffusion burn rates are faster than the kinetic rates, it can be concluded that the lead will burn at those rates. Equation 3.6 shows the burn rate proposed by Yetter and Dryer for metal droplet combustion.

$$t_b = \frac{\rho_p d_0^2}{8\rho_O D\, ln(1+iY_{O,\infty})} \tag{3.6}$$

$$D = 0.176\left(\frac{T}{298}\right)^{3/2} \tag{3.7}$$

In Equation 3.6, t_b is the droplet burn time, ρ_p is the lead particle density, d_0 is the droplet diameter, ρ_O is air density, D is the oxidizer diffusion through Nitrogen found in Equation 3.7 with T in Kelvin, i is the fuel to air ratio (3.02 at stoichiometric conditions), and $Y_{O,\infty}$ is the mass fraction of oxidizer in the freestream far away from the reaction (0.233 in air). Using this equation and the same 10 micron droplet at 1300 C from the kinetic burn rate calculations, the burn time is 5.2 milliseconds. Lowering the temperature to 1250 C only increases the burn time to 5.3 milliseconds. This is an order of magnitude smaller than the kinetic rate. Even if the extrapolation used for the kinetic data overestimated the actual burn rate, it is unlikely that it overestimated by more than an order of magnitude. Since the diffusion rate is so much faster, this is a strong enough conclusion to assume that the oxidation rate of lead is diffusion controlled. Figure 3.3 displays kinetic vs

diffusion burn rates at 900 K to show the scale difference. Figures 3.4 and 3.5 show burn rates of lead droplets based on droplet size and temperature for a diffusion controlled reaction.

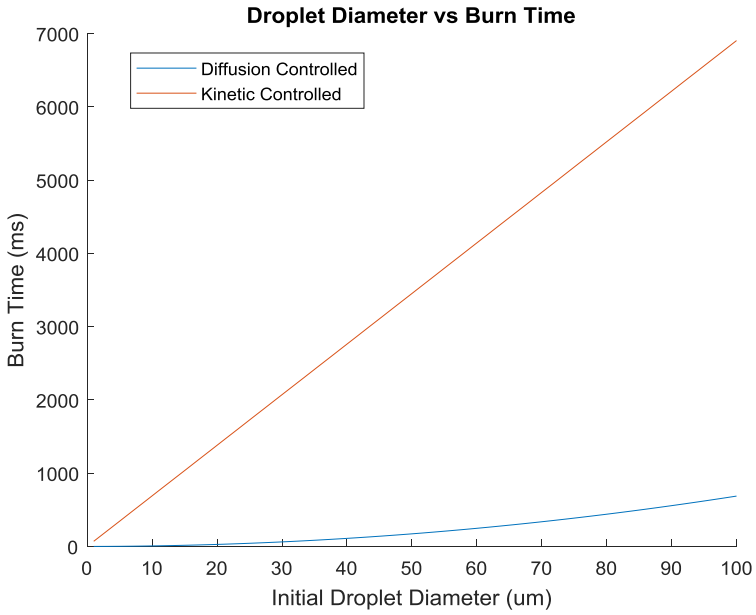

Figure 3.3 Kinetic vs Diffusion Burn Rates

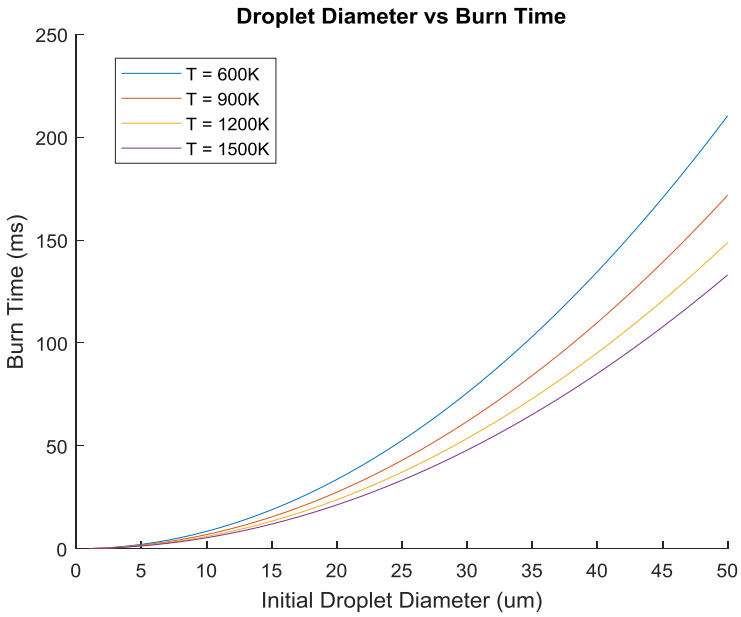

Figure 3.4 Large Lead Droplet Burn Rates

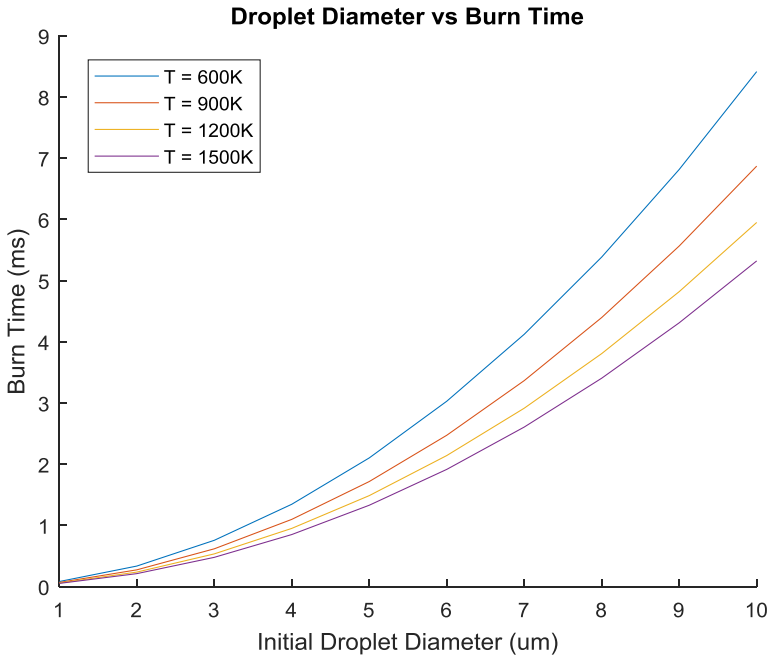

Figure 3.5 Small Lead Droplet Burn Rates

As seen above, the temperature doesn't play a large factor in the diffusion burn rates for lead droplets because the diffusivity does not change greatly with temperature. This is actually extremely helpful in the design of the combustion chamber. Recall from Section 1.3 that lead oxide has two different forms, tetragonal and orthorhombic [7]. The desired form of the lead oxide is a tetragonal crystal structure which is only formed below 762 K [2]. Figure 3.4 shows that the droplets will still oxidize extremely quickly at this lower temperature. Keeping the temperature low is also good as many metal oxides suffer from dissociation at high temperatures [9]. The dissociation temperature of lead oxide has not been empirically tested, but keeping the temperature below 762 K ensures that the lead oxide stays below its dissociation temperature. However, Figure 3.3 shows that diffusion controlled burn rates rely heavily on droplet diameter. In order to keep a combustion chamber at a reasonable length, atomization of the lead spray must be prioritized. Using 300 ft/s air speeds that were previously tested at the Barton pot, each millisecond of burn time adds 3.6 inches to the combustor.

3.3 Oxidation Temperature Control

Since the data shows that lead oxidation will occur rapidly even at temperatures below 762 K, the temperature of a combustion chamber must be regulated. The Barton pot utilizes water addition in order to keep the temperature below 762 K. Discovered in empirical trials, water must be added as an inert substance to facilitate the lead oxidation [7]. For the combustor, water will be added into the air upstream of the injector in order to control the temperature. The Barton pot adds water to the reaction zone in the same manner. The following equation shows the chemical reaction of lead oxide.

$$Pb + \frac{1}{2}(O_2 + 3.76N_2) + aH_2O \rightarrow PbO + 1.88N_2 + aH_2O \qquad (3.8)$$

The value of a is determined by the desired temperature of the reaction. To determine the adiabatic flame temperature of reaction, an enthalpy balance is used. Equation 3.9 shows the enthalpy balance setup.

$$\left(\bar{h}_f^o + \Delta h\right)_{Pb,r} + \frac{1}{2}\left(\bar{h}_f^o + \Delta h\right)_{O_2,r} + 1.88\left(\bar{h}_f^o + \Delta h\right)_{N_2,r} + a\left(\bar{h}_f^o + \Delta h\right)_{H_2O,r} =$$

$$\left(\bar{h}_f^o + \Delta h\right)_{PbO,p} + 1.88\left(\bar{h}_f^o + \Delta h\right)_{N_2,p} + a\left(\bar{h}_f^o + \Delta h\right)_{H_2O,p} \qquad (3.10)$$

Equations for each value of enthalpy change are recorded in the MATLAB section of the appendix. Plugging in the values for each term and using 0 for the value of a, the adiabatic flame temperature comes out to approximately 1900 K. Since this is much higher than the tetragonal crystal temperature cap of 762 K, water will obviously be necessary to cool the system. To determine the amount of water needed, water was first added to equation 3.9.

With Equation 3.4 the moles of water needed per mole of lead can be determined. Using the desired temperature, all of the Δh terms can be replaced with equations for enthalpy with respect

to temperature from the National Institute of Standard and Technology. With a given input temperature, the only unknown becomes a. Equation 3.11 shows the resulting calculation.

$$a = \left[(\Delta h)_{Pb,r} - \left(\bar{h}_f^o + \Delta h\right)_{PbO,p} + 1.88(\Delta h)_{N_2,p}\right] / (\Delta h)_{H_2O,p} \quad (3.11)$$

Equation 3.11 is made by removing all of the enthalpy of formation terms for the molecules that do not have enthalpy of formations. It also assumes that the air and water enters the combustion chamber at 298 K. For any other temperatures of air and water, the enthalpy change of those substances on the reactants side would need to be included in Equation 3.11. For a sample calculation assuming air and water enter at 298 K, lead enters at 650 K, with lead and air flowrate of 6000 lbs/hr and 1 lb/s respectively, the necessary amount of water to keep the reaction below 762 K is 1.129 lbs/s or 8.12 GPM. The amount of water can be adjusted to let the temperature rise above 762 K if orthorhombic crystals of lead oxide were desired.

3.4 Combustion Chamber Design Process

The Barton reactor has numerous limitations as the atomization mechanism and particle residence time are poorly controlled. For many applications, lead oxide produced in the reactor must be subsequently milled to meet particle size requirements for customers. The reactor and milling processes demand substantial floor space and capital investment. For these reasons, it would be desirable to ultimately develop an in-line combustion process where the atomization and combustion occur in a tube/pipe. Substantially higher production rates and greatly reduced footprints (and hence capital investment) would be required. If atomizer design can be improved to control particle sizes, post-combustion milling processes might be simplified or removed altogether. In short, there are many factors motivating the development of an in-line system. Figure 3.6 below shows a diagram of what such a system would look like.

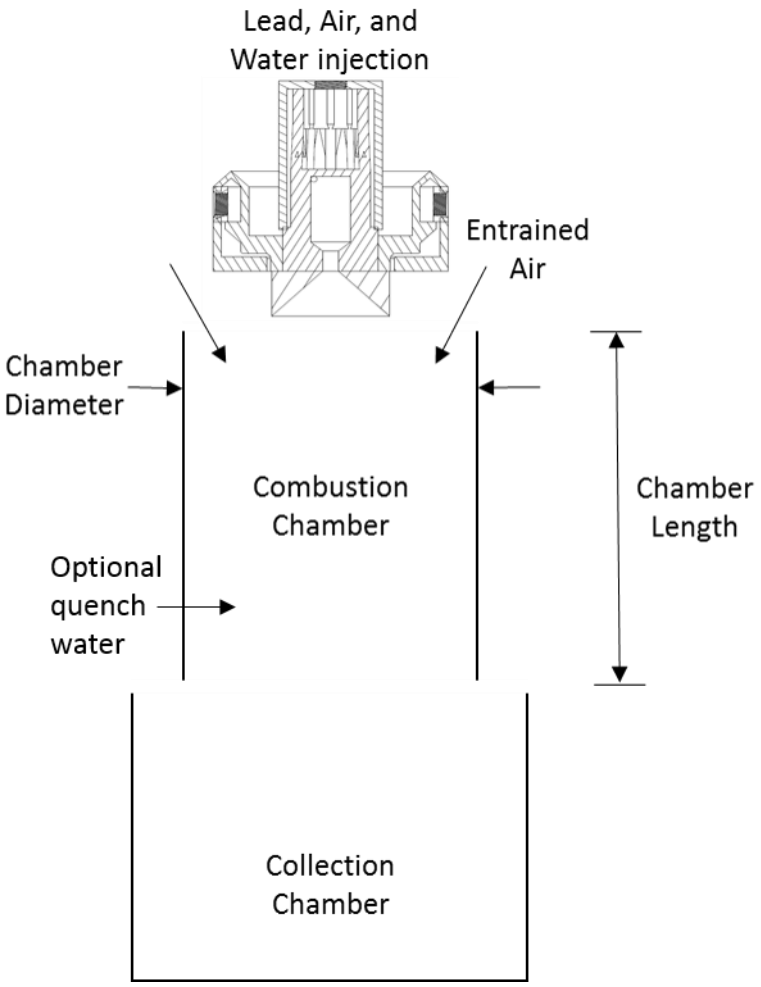

Figure 3.6 In-Line Lead Combustor Design

Once all the previous calculations are complete, the combustion chamber can be designed. The injection portion of the combustion chamber is designed using the process described in detail in Chapter 2. The diameter of the combustion chamber is a variable dimension as it does not directly have an effect on any of the calculations. However, if it is allowed to get large enough that the droplets on the edge of the spray experience a lower temperature than the droplets in the center, they could oxidize at a slow enough rate they may exit the combustor before oxidation is completed. This is an unlikely scenario due to the earlier discussed fact of temperature not playing a large role in the oxidation rate of the droplets.

The main factor in the diameter of the chamber is the desire to keep lead droplets from hitting the walls of the chamber and freezing. In order to help combat this, a ring of entrained air was added to the combustion chamber design. Using the measured values of vacuum pressure pulled by the injection of air, the amount of air entrained can be calculated. This air is assumed to be so much lower than the injected air, it will not be factored into the oxidation calculations. The point of this air is to flow along the walls of the chamber and keep the walls cool and free of any lead particles that drift too close to them. None of this air will be used for combustion.

The most important part of the combustion chamber is the length. The length will determine how long the droplets of lead will have to oxidize. Varying the length of the chamber could theoretically stop oxidation early if a lower oxidized portion of lead was desired. For example, many industrial applications of lead oxide prefer only 80-85% of the lead to be oxidized [1]. Shortening the combustion chamber to 80-85% of its calculated necessary length for 100% oxidation would ensure only 80-85% of the lead was oxidized as long as the lead oxide was quenched immediately upon exiting the chamber.

To calculate the length of the combustor, the speed of air and lead is combined using the total momentum ratio (TMR) of air to lead calculated using Equation 3.12.

$$TMR = \frac{\dot{m}_{air} v_{air}}{\dot{m}_{Pb} v_{Pb}} \tag{3.12}$$

The speed of the droplets is them calculated using Equation 3.13.

$$v_{droplets} = \frac{TMR}{TMR+1} v_{air} + \frac{1}{TMR+1} v_{Pb} \tag{3.13}$$

Once the droplets velocity is calculated, the length of the combustion chamber is simply the droplet velocity multiplied by the burn time calculated in Section 3.2 and shown in Equation 3.14.

$$L_{chamber} = v_{droplets} * t_{burn} \tag{3.14}$$

Once the length of the combustion chamber is set, the amount of variability is limited. If more water is added, the temperature will decrease and slow down the oxidation rate. Since the combustor length is set, this will lead to the droplets not fully oxidizing. The amount of oxidation would scale with droplet surface area. The temperature would have to be reduced significantly to make a large percentage change in the amount of oxidation. Since the lowest temperature lead will stay liquid at is 600 K, if the design point is below 762 K, the temperature cannot be lowered enough to reduce oxidation to 80-85% as required by some processes. For this level of oxidation a separate chamber would likely need to be designed.

However, the temperature can be raised without limit as this would speed up oxidation. There is no downside to fully oxidized particles staying in the chamber for longer than needed. This points to the design condition for a chamber to fit all needs would be to design a chamber long enough for the lowest temperature requirement. Once designed and installed, the combustion chamber could simply open into a collection chamber for the lead oxide particles similar to the one that the current Barton pot system empties into [7]. This type of lead oxide production process wasn't constructed and tested, but it is a possible replacement for the Barton pot process. Since lead will oxidize rapidly at small particle sizes a combustor system is the ideal process for producing lead oxide due to its simplicity. The next sections discusses results and shows graphs of the impact of changing various factors in the chamber.

3.5 Results and Operation Parameters of Combustion Chamber

The combustion chamber has many different parameters to control its design and operation. In order to keep all of these factors in mind when designing a combustion chamber, an Excel tool was created that designs an injector and chamber design based on input parameters. The main inputs are flowrates of lead and air; lead, air, and chamber temperature; lead and air feed pressures; and number of injection sites. An image of the tool is shown below in Figure 3.7.

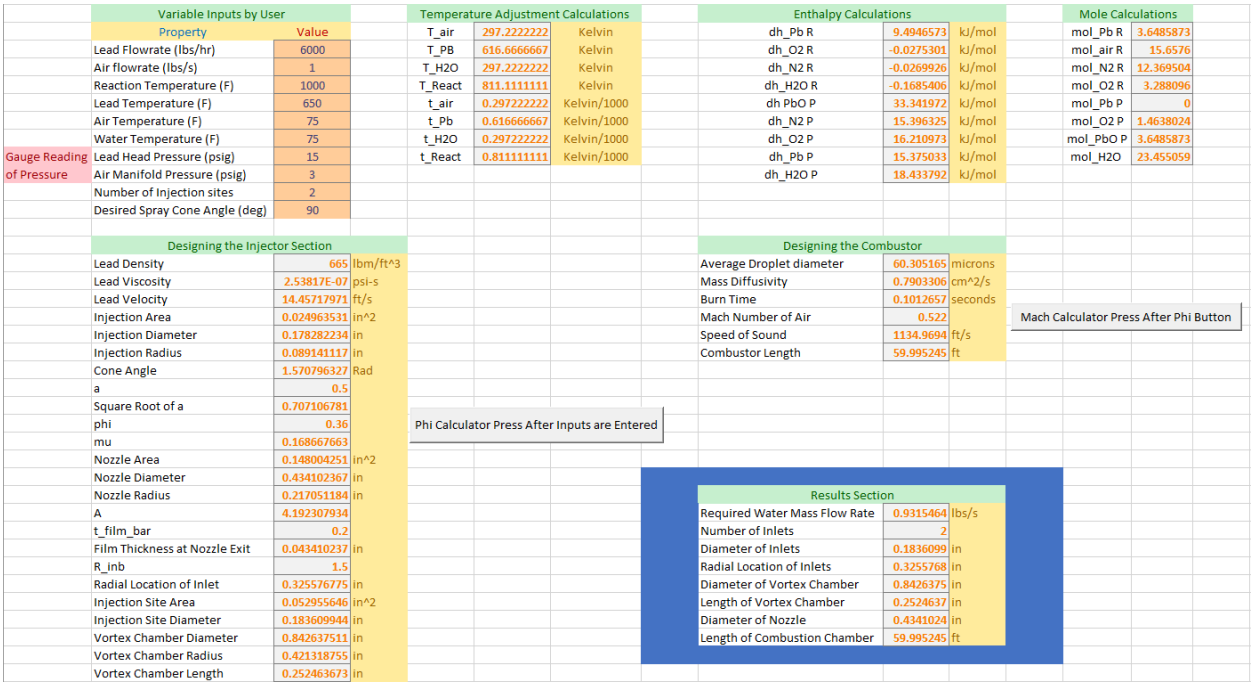

	Variable Inputs by User		
	Property	Value	
	Lead Flowrate (lbs/hr)	6000	
	Air flowrate (lbs/s)	1	
	Reaction Temperature (F)	1000	
	Lead Temperature (F)	650	
	Air Temperature (F)	75	
	Water Temperature (F)	75	
Gauge Reading	Lead Head Pressure (psig)	15	
of Pressure	Air Manifold Pressure (psig)	3	
	Number of Injection sites	2	
	Desired Spray Cone Angle (deg)	90	

Temperature Adjustment Calculations		
T_air	297.2222222	Kelvin
T_PB	616.6666667	Kelvin
T_H2O	297.2222222	Kelvin
T_React	811.1111111	Kelvin
t_air	0.297222222	Kelvin/1000
t_Pb	0.616666667	Kelvin/1000
t_H2O	0.297222222	Kelvin/1000
t_React	0.811111111	Kelvin/1000

Enthalpy Calculations		
dh_Pb R	9.4946573	kJ/mol
dh_O2 R	-0.0275301	kJ/mol
dh_N2 R	-0.0269926	kJ/mol
dh_H2O R	-0.1685406	kJ/mol
dh PbO P	33.341972	kJ/mol
dh_N2 P	15.396325	kJ/mol
dh_O2 P	16.210973	kJ/mol
dh_Pb P	15.375033	kJ/mol
dh_H2O P	18.433792	kJ/mol

Mole Calculations	
mol_Pb R	3.6485873
mol_air R	15.6576
mol_N2 R	12.369504
mol_O2 R	3.288096
mol_Pb P	0
mol_O2 P	1.4638024
mol_PbO P	3.6485873
mol_H2O	23.455059

Designing the Injector Section		
Lead Density	665	lbm/ft^3
Lead Viscosity	2.53817E-07	psi-s
Lead Velocity	14.45717971	ft/s
Injection Area	0.024963531	in^2
Injection Diameter	0.178282234	in
Injection Radius	0.089141117	in
Cone Angle	1.570796327	Rad
a	0.5	
Square Root of a	0.707106781	
phi	0.36	
mu	0.168667663	
Nozzle Area	0.148004251	in^2
Nozzle Diameter	0.434102367	in
Nozzle Radius	0.217051184	in
A	4.192307934	
t_film_bar	0.2	
Film Thickness at Nozzle Exit	0.043410237	in
R_inb	1.5	
Radial Location of Inlet	0.325576775	in
Injection Site Area	0.052955646	in^2
Injection Site Diameter	0.183609944	in
Vortex Chamber Diameter	0.842637511	in
Vortex Chamber Radius	0.421318755	in
Vortex Chamber Length	0.252463673	in

Phi Calculator Press After Inputs are Entered

Designing the Combustor		
Average Droplet diameter	60.305165	microns
Mass Diffusivity	0.7903306	cm^2/s
Burn Time	0.1012657	seconds
Mach Number of Air	0.522	
Speed of Sound	1134.9694	ft/s
Combustor Length	59.995245	ft

Mach Calculator Press After Phi Button

Results Section		
Required Water Mass Flow Rate	0.9315464	lbs/s
Number of Inlets	2	
Diameter of Inlets	0.1836099	in
Radial Location of Inlets	0.3255768	in
Diameter of Vortex Chamber	0.8426375	in
Length of Vortex Chamber	0.2524637	in
Diameter of Nozzle	0.4341024	in
Length of Combustion Chamber	59.995245	ft

Figure 3.7 Combustion Chamber Design Tool

The tool takes inputs in the top left section of the Excel sheets and then solves for all of the outputs displayed in orange in the light gray boxes. The processes for determining all of the values has been shown in the earlier chapters of this paper except for finding the average droplet diameter. The droplet diameters were calculated using a formula for Sauter Mean Diameter developed by Rizkalla and Lefebvre shown below in Equation 3.15 [5].

$$SMD = 3.33 * 10^{-3} \frac{(\sigma \rho_L t)^{0.5}}{\rho_A U_A}\left(1 + \frac{\dot{m}_L}{\dot{m}_A}\right) + 13 * 10^{-3}\left(\frac{\mu_L^2}{\sigma \rho_L}\right)^{0.425} t^{0.575}\left(1 + \frac{\dot{m}_L}{\dot{m}_A}\right)^2 \quad (3.15)$$

In Equation 3.15 σ is the surface tension of lead equal to 0.00251 pounds per inch [6], ρ is the density with subscripts L and A for lead and air respectively, t is the film thickness, μ is the lead viscosity equal to 2.54e-7 psi-s [3], and $\dot{m}$ is the mass flowrate. This formula is only an approximation, as it was derived for kerosene as the working fluid [4], but the type of spray it was derived for is the same as produced by the injector described within this paper. As seen in Figure 3.6, the resulting SMD is about 60 microns with these inputs. This droplet size would require a 60 ft long combustion chamber. Since this is not very practical, minimizing the droplet size would be critical in the operation of such a combustion chamber. Graphs later in this section show how changing certain parameters can change droplet size. Because SMD data for lead is not readily available, empirical testing of the injector with an airblast would be required to determine the true SMD of the resulting droplets. The MATLAB code used to solve for the other values is attached in the appendix.

This process was designed to allow a user to vary the properties of the produced lead oxide. Lead oxide has many uses, and each use requires a slightly different version of it. The main variation required is percent oxidation. With a combustion chamber this could be variable by adjusting many different parameters. Simply ending the chamber at the desired oxidation point is the simplest solution, but to be able to use on chamber to produce a variety of oxides, it is desired to know the effect of changing certain input parameters. The following sections show the result to the system caused by the change in some of these parameters.

3.6 Temperature Change Factors

The following graphs show the impact to combustion temperature change resulting from various condition changes. Figure 3.8 uses 75F air at 1 lb/s, 2 psig and 650F lead at 6000 lb/hr or 1.667 lb/s, 15 psig. As seen in the figure, the temperature of the water does not have a large impact on the reaction temperature. While the difference between 40 F and 150 F could be significant at lower reaction temperatures, if the water varies a few degrees during operation, it will not affect the system.

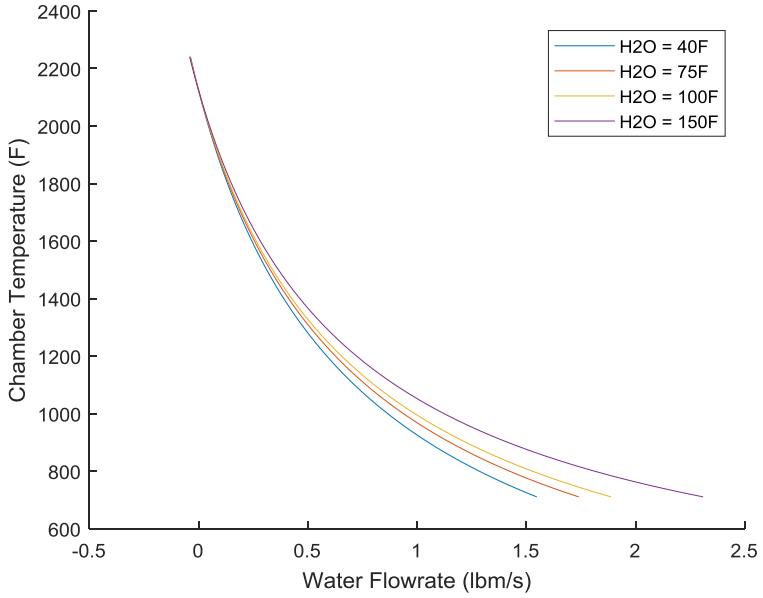

Figure 3.8 Water Flowrate vs Chamber Temperature

Figure 3.9 uses air and water at 75F, 2 psig, with lead at 650F and 6000 lb/hr, 15 psig. The figure below shows that air flowrate has a significant impact on the chamber temperature and thus the required water flowrate. If it is cheaper to add additional air to the system instead of water, that should be taken advantage of. Having higher than stoichiometric amounts of air will also decrease

the adiabatic flame temperature of the reaction which reduces the maximum temperature the reaction can reach.

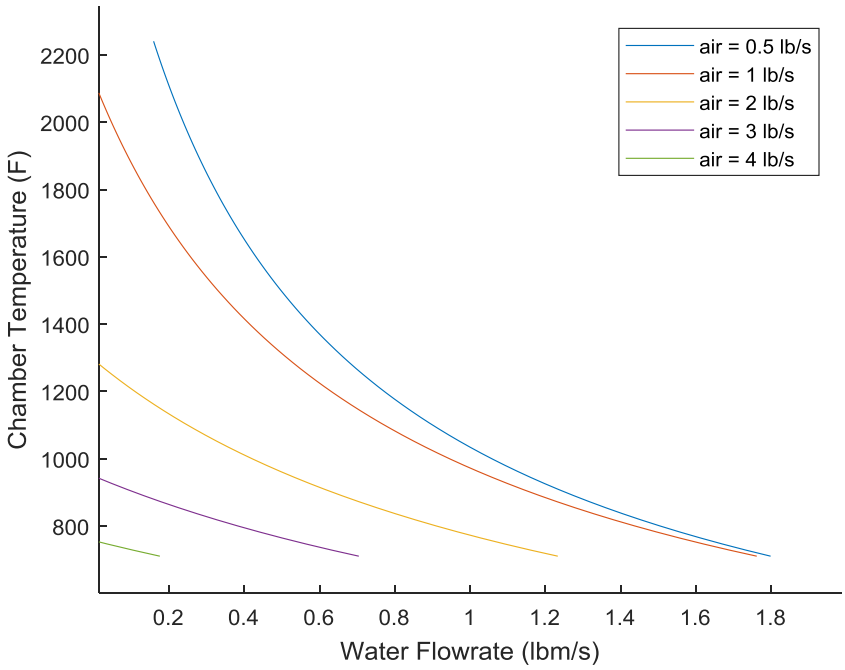

Figure 3.9 Water Flowrate vs Chamber Temperature

3.7 Droplet Size Factors

The following graphs show the impact to droplet size resulting from various condition changes. Because droplet size is the determining factor in the burn rates and the overall design of the combustion chamber, many scenarios are run in order to determine the effects of each input.

Figure 3.10 below uses air at 75F, 2 lb/s, 3 psig and lead at 650F. Water added has a negligible effect on droplet size and is thus neglected. As seen in the below figure, lead pressure plays a large role in droplet size. There is a very direct correlation in increasing the lead pressure to reduce droplet size. A certain combustor design will have a maximum droplet size that is able to

completely burn while inside and that will be limited by the amount of lead pressure that can be generated. The more pressure the lead is fed with, the higher that flowrates can be raised while staying under that maximum lead droplet diameter.

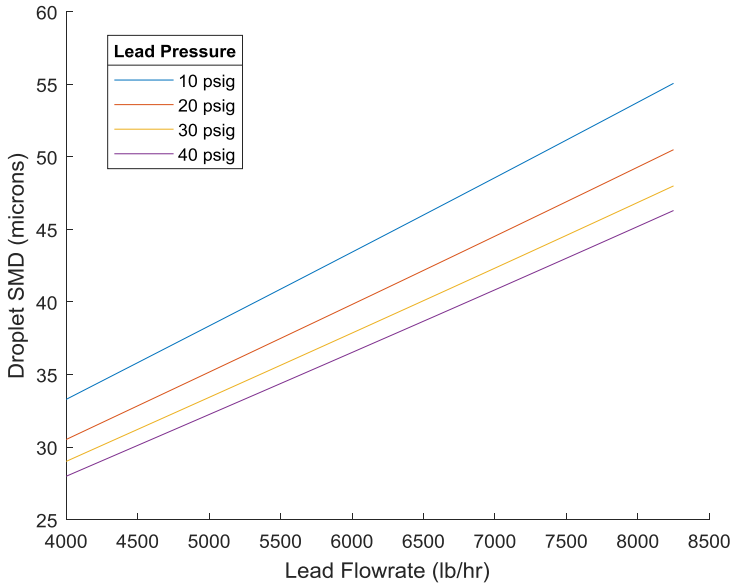

Figure 3.10 Lead Flowrate vs Droplet Size

Figure 3.11 below uses air at 75F; and lead at 650F, 30 psig, 6000 lb/hr. While nothing can be done to lower desired lead flow, the amount of air and pressure should be used to minimize droplet size. As seen above in Figure 3.8, additional air has the benefit of lowering the reaction temperature, so less water is needed to maintain temperature. The graph starts at 0.5 lb/s of air because that is the stoichiometric amount of air for 6000 lb/hr of lead. The results show that increasing that to at least 1.5 lb/s significantly reduces droplet size. Because decreasing droplet size is the most important factor in the combustor, the highest air pressure the system is able to generate should be used.

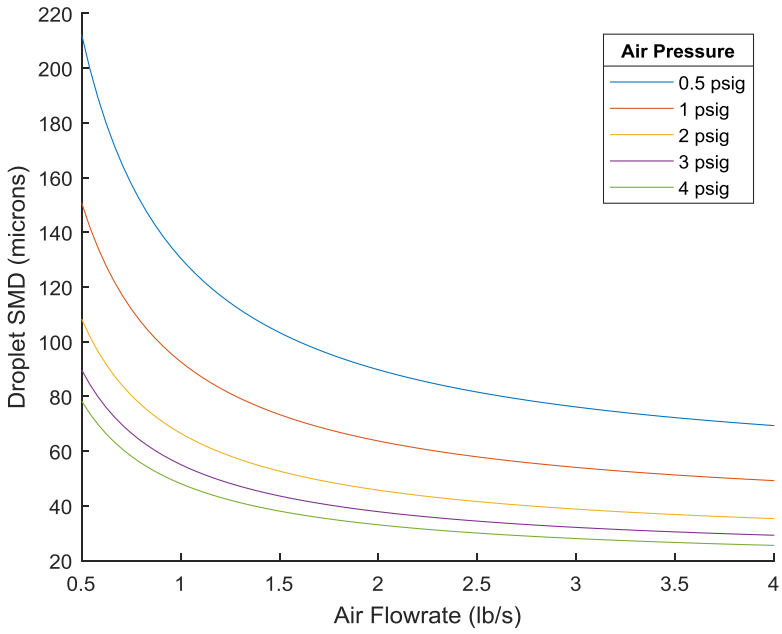

Figure 3.11 Air Flowrate vs Droplet Size

Figure 3.12 below shows the effect of droplet size on combustor length for an operation temperature of 900 K; 6000 lb/hr lead at 615 K, 15 psig; 1 lb/s air at 300 K, 2 psig. Droplet diameter is the leading factor of combustor length. It needs to be minimized in order to produce a realistic combustor. Having a combustor that is over 20 feet long is not practical to operate inside of a factory and would not be smaller than the current Barton pot system. Based on the results from Figure 3.12, the droplet size must be under 30 microns to keep the combustor under 20 ft. The previous figures show the importance of head pressure in droplets size. Maximizing the pressure of air and lead will help get the particle size as small as possible. Using the Excel tool developed to design a combustor, the parameters were altered using the results from the previous figures in order to minimize the droplet size.

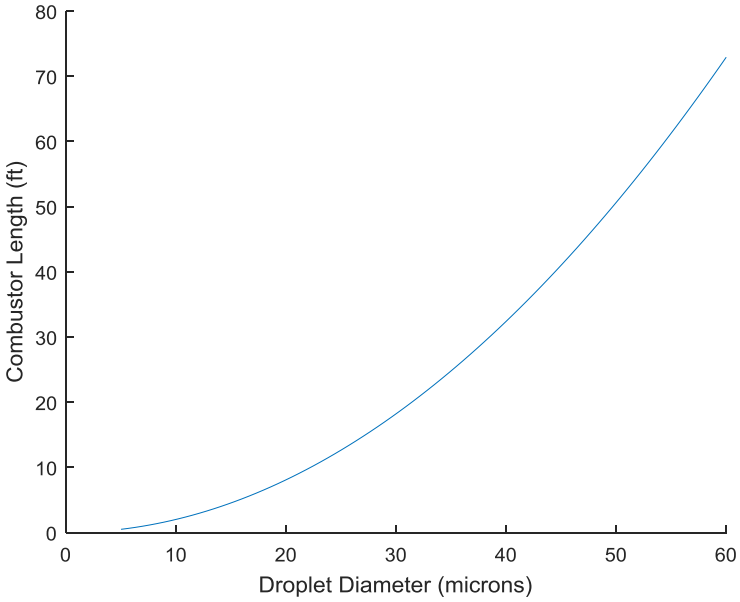

Figure 3.12 Droplet Diameter vs Combustor Length

Finding the "best" operating conditions is not possible due to always being able to increase performance by increasing air and lead pressures, and air flowrate. However, it will eventually become too costly to continue to increase these inputs. Using a reaction temperature of 900 K, 2 lb/s of 300 K air at 4 psig, 6000 lb/hr of 615 K lead at 30 psig, gives an average droplet size of 33 microns and a combustor length of 18 ft. Increasing the pressures will decrease droplet size and further reduce the length of the combustor. In order to get the droplets down to 10 microns and remove the milling process, very high pressures of lead and air would be required. A cost benefit analysis would be required to determine how high the pressures could be raised while keeping the pressure costs lower than milling costs. If lead oxide with an orthorhombic crystal structure was desired, the reaction temperature could be greatly raised and further reduce the length of the combustor by reducing the burn time of the lead droplets. This combustor designs flexibility of operation shows its potential superiority to the Barton pot process.

Purely looking at production benefits, the optimized combustor designed in the previous paragraph was given to be 18 ft with a droplet diameter of 33 microns at a production rate of 6000 lb/hr of lead. If the pressures of lead and air are held constant, and the flowrates of lead and air are doubled, the particle diameter raises to 41 microns and the length only increases to 24 ft. The diameter increase does not affect the product at a production standpoint as they will both require milling. However, for just an extra 6 feet in length, the combustor would be able to handle twice the flowrate. For each combustor built, it could handle the flowrate of two Barton pots. The amount of factory space and energy saved would make the lead combustor much more valuable in the long run than the Barton pot system.

3.8 Chapter 3 References

[1] Kelley, Barry P. “Lead-Acid Battery Manufacture.” *ILO Encyclopaedia of Occupational Health and Safety*, 16 Mar. 2011, www.iloencyclopaedia.org/component/k2/item/661-lead-acid-battery-manufacture.

[2] Malcolm W. Chase, Jr. (1998). NIST-JANAF thermochemical tables. “JANAF Table Data for PbO.” Washington, DC : New York :*American Chemical Society ; American Institute of Physics for the National Institute of Standards and Technology*,

[3] Ofte, D. “The Viscosities of Liquid Uranium, Gold and Lead.” *Journal of Nuclear Materials*, vol. 22, no. 1, 1967, pp. 28–32., doi:10.1016/0022-3115(67)90105-5.

[4] Omer, K, and N Ashgriz. “Spray Nozzles.” *Handbook of Atomization and Sprays*, Springer, 2016, pp. 497–579.

[5] Rizkalla, A., and Lefebvre, A. H., The Influence of Air and Liquid Properties on Air Blast Atomization, *ASME J. Fluids Eng.*, Vol. 97, No. 3, 1975, pp. 316-320.

[6] Schwaneke, Alfred E., and Wilbert L. Falke. “Surface Tension and Density of Liquid Lead.” *Journal of Chemical & Engineering Data*, vol. 17, no. 3, 1972, pp. 291–293., doi: 10.1021/je600

[7] Vahrenkamp, G., Manor, S., & Coppersmith, F.; National Lead Company, assignee. Process for Producing Lead Oxides. *U.S. Patent No. 3,322,496.* May 30, 1967.

[8] Weyand, Thomas Edward, "The oxidation kinetics of liquid lead and lead alloys" (1970). *Doctoral Dissertations*. 2042. http://scholarsmine.mst.edu/doctoral_dissertations/2042

[9] Yetter, Richard A., Dryer, Frederick L. “Metal Particle Combustion and Classification.” *Microgravity Combustion: Fire in Free Fall,* Academic Press, 2001, pp. 419-478.

CHAPTER 4. CONCLUSIONS

4.1 Summary and Conclusions

The Barton pot is the current best method of producing lead oxides. This paper has described in detail the process of improving the Barton pot in terms of production rate, oxidation time, and particle size. The end goal of the process is to reduce the particle size enough, so the lead oxide does not require milling after leaving the Barton pot. To this end, many injectors were designed and tested to determine a better process for lead input to the Barton pot than the current method of lead pouring in through a channel.

After prototyping and testing, the swirl injector was selected as the best choice for the atomization of lead inside the Barton pot. The swirl injector has the benefit of operating with as few as two injection sites. This allows for the largest area of injection. Large injection area is a benefit because lead flows poorly through extremely small orifices. A pintle injector, for example, requires many more orifices and would thus result in too small a flow area to work for lead. Using a swirl injector combined with the current method of atomization, a propeller blade and baffle plate, should reduce the particle size and residence time enough to allow for higher flowrates and the removal of the milling process.

While improving the Barton pot process was the main goal of this research, it was taken a step further looking into alternative ways of producing the lead oxide. Before that, more information on the actual combustion of lead was necessary. To determine burn rates of lead, kinetic data was examined and extrapolated to be compared to diffusion controlled burn rates. Through this study,

it was determined that the oxidation time of lead droplets was a diffusion controlled reaction and could thus be modeled using the d-squared law.

Once a method for burn rate was set, a simple rocket-style combustion chamber was designed for lead. The injection system used was the swirl injector that was designed for the Barton pot. Since the Barton pot atomization methods are not present, an airblast was added to the injector in order to atomize the sheet of lead spraying from the swirl injector. Water is added to control the temperature inside the reaction chamber. An Excel tool was designed to take input conditions such as lead and air flowrates and create an injector and combustion chamber design using the burn rate of droplets and predicted droplet size.

4.2 Future Work

The graphs in the previous sections were all created through theoretical predictions. Testing of the injector with lead and varying the inputs would be required to verify the droplet size predictions. Running tests and gathering droplet data with a PDPA system would help understand the accuracy of the predictions. Lead oxide particle sizes are desired to have a nice mix of sizes between 1 and 10 microns. The current Barton pot production method requires the lead oxide to be milled into these smaller particle sizes. The data shows that it is possible the combustion chamber lead oxide production method will also require this milling. However, the combustion chamber holds the benefit of being able to handle lead flowrates much higher than the Barton pot. Even if particle sizes still require milling after exiting the chamber, the production benefits could be worth implementing the design.

APPENDIX

MATLAB CODE

Lead Enthalpy Calculations from NIST

```
%% Lead Enthalpy Calculation from NIST Website

T = input('Input Lead Temperature(K): '); %Get desired lead temperature
t = T/1000;
A = 38.00449;
B = -14.62249;
C = 7.255475;
D = -1.033370;
E = -0.330775;
F = -7.944328;
G = 118.7992;
H = 4.282993;
dH = A*t + B*((t^2)/2) + C*((t^3)/3) + D*((t^4)/4) - E/t + F - H; %Enthalpy
Calculation
dH = dH*1000/207.2; %conversion to kJ/kg
```

Lead Oxide Enthalpy Calculations from NIST

```
%% Lead Oxide Enthalpy Calculation from NIST Website

T = input('Input Lead Oxide Temperature(K): '); %Get lead oxide temperature
t = T/1000;
A = 65.00221;
B = -0.003325;
C = 0.001718;
D = -0.000297;
E = -0.000306;
F = -221.6307;
G = 152.039;
H = -202.2491;
dH = A*t + B*((t^2)/2) + C*((t^3)/3) + D*((t^4)/4) - E/t + F - H; %Calculate
Enthalpy
dH = dH*1000/223.2; %Convert to kJ/kg
```

Burn Time Rate Estimations Using Previous Kinetic Data

```
%% Calculate Oxidation Time Based on Droplet Size
clear;
clc;
Tk = input('Enter temperature (K): '); %Environment Temperature
T = Tk - 273.15; %Conver to Celcius
D = input('Enter droplet diameter (microns): '); %droplet size
%% Get constants for oxidation equation
%Interpolate between equations given in Oxidation reference
```

```
if T < 345
    disp('Enter a temperature greater than 345 deg Celsius');
elseif T >= 345 && T < 392
    c1 = ((T-345)/(392-345))*(-0.016+0.006)+(-0.006); %First eq constant
    c2 = ((T-345)/(392-345))*(0.04-0.017)+0.017; %Second eq constant
elseif T >= 392 && T < 439
    c1 = ((T-392)/(439-392))*(-0.026+0.016)+(-0.016); %First eq constant
    c2 = ((T-392)/(439-392))*(0.065-0.04)+0.04; %Second eq constant
elseif T >= 439 && T < 488
    c1 = ((T-439)/(488-439))*(-0.06+0.026)+(-0.026); %First eq constant
    c2 = ((T-439)/(488-439))*(0.138-0.065)+0.065; %Second eq constant
elseif T >= 488 && T < 532
    c1 = ((T-488)/(532-488))*(-0.114+0.06)+(-0.06); %First eq constant
    c2 = ((T-488)/(532-488))*(0.255-0.138)+0.138; %Second eq constant
elseif T >= 532 && T < 580
    c1 = ((T-532)/(580-532))*(-0+0.114)+(-0.114); %First eq constant
    c2 = ((T-532)/(580-532))*(0.334-0.255)+0.255; %Second eq constant
% If temperature is greater than 580 C (maximum in reference)
%Linearly interpolate out past that line
elseif T >= 580 && T <= 1300
    c1 = ((T-580)/(1300-580))*(-1317+0)+0; %First
    c2 = ((T-580)/(1300-580))*(5490-.334)+0.334; %Second
else
    disp('Enter a temperature under 1300 Celsius');
end
%% Calculate how much mass of oxygen is needed
V = (4/3)*pi*(((D/1000)/2)^3); %volume of drop in mm^3
m_Pb = 10.65*V; %mg of lead
mol_Pb = m_Pb/207200; %mol of lead and mol of oxygen
mol_O = .5*mol_Pb; %mol of Oxygen per mol of lead for stoichimetric ratio
m_O = 15999.4*mol_O; %mg of oxygen needed for oxidation of droplet
%% Calculate time of oxidation
SA_Pb = (4*pi*((D/10000)/2)^2); %surface area of droplet in cm^2
Ratio = m_O/SA_Pb; %mg oxygen/cm^2 of lead
t = 0; %oxidation time seconds
while Ratio > (c1*((t/3600)^2) + c2*(t/3600))
    t = t + 0.001; %increment burn time in seconds
end
milli = t * 1000; %Final burn time in milliseconds
fprintf('The time to burn a %1.0f micron droplet at %1.0f deg K is %1.0f
milliseconds\n'...
    ,D,Tk,milli);

%% Yetter Ref method
%Calculate burn time for secondary method
tb = 8.803 + ((2024-Tk)/(2024-600)*(10.678-8.803));
```

Design of Swirl Injector and Combustion Chamber

```
%% Ultimate_Combustor
clear all;
% Input desired flowrates for lead and temperature
mdot_Pb = 6000; %Lead flowrate in lb/hr
T = 1000; %Temperature of Reaction in K
TF = (9/5).*(T-273)+32; %Temperature converted to F
```

```
t = T./1000; %Constant used for enthalpy calculations
Tair = 300; %Air input Temperature
tair = Tair/1000; %Constant used for enthalpy calculations
TPb = 615; %Lead input temperature
tPb = TPb/1000; %Constant used for enthalpy calculations

figure(1)
hold on

for mdot_air = [1] %Air Flowrate in lb/s

    TH2O = 300; %Water input Temperature K
    tH2O = TH2O/1000; %Constant used for enthalpy calculations

    %Use Temperature to calculate how much water is needed
    %First determine all enthalpy values
    %r for reactant value, p for product value

    dhPbr = 38.00449*tPb + (-14.62249)*((tPb^2)/2) + 7.255475*((tPb^3)/3)...
        + (-1.03337)*((tPb^4)/4) - (-0.330775/tPb) + (-12.227321);

    dhO2r = 31.32234*tair + (-20.23531)*((tair^2)/2) +
57.86644*((tair^3)/3)...
        + (-36.50624)*((tair^4)/4) - (-0.007374/tair) - 8.903471;

    dhN2r = 28.98641*tair + (1.853978)*((tair^2)/2) + (-
9.647459)*((tair^3)/3)...
        + (16.63537)*((tair^4)/4) - (0.000117/tair) - 8.671914;

    dhH2Or = (-203.6060)*tH2O + (1523.29)*((tH2O^2)/2) + (-
3196.413)*((tH2O^3)/3)...
        + (2474.455)*((tH2O^4)/4) - (3.855326/tH2O) + 29.1826;

    dhPbOp = 65.00221.*t + (-0.003325).*((t.^2)./2) +
0.001718.*((t.^3)./3)...
        + (-0.000297).*((t.^4)./4) - (-0.000306./t) - 19.3816;
    dhN2p = 19.50583.*t + (19.88705).*((t.^2)./2) + (-
8.598535).*((t.^3)./3)...
        + (1.369784).*((t.^4)./4) - (0.527601./t) - 4.935202;

    dhO2p = 30.03235.*t + (8.772972).*((t.^2)./2) + (-
3.988133).*((t.^3)./3)...
        + (0.788313).*((t.^4)./4) - (-0.741599./t) - 11.32468;

    dhPbp = 38.00449.*t + (-14.62249).*((t.^2)./2) + 7.255475.*((t.^3)./3)...
        + (-1.03337).*((t.^4)./4) - (-0.330775./t) + (-12.227321);

    dhH2Op = 30.092.*t + (6.832514).*((t.^2)./2) + (6.793435).*((t.^3)./3)...
        + (-2.534480).*((t.^4)./4) - (0.082139./t) - 9.0546;

    %Find amount of moles of Lead and Air
    mol_Pbr = (mdot_Pb./3600).*2.189152365;
    mol_airr = mdot_air.*15.6576;
```

```
    %Separate air into element moles
    mol_N2 = mol_airr.*0.79;
    mol_O2r = mol_airr.*0.21;

    %Calculate if excess Oxygen or Lead in Products
    if mol_Pbr <= 2.*mol_O2r
        mol_Pbp = 0;
        mol_O2p = mol_O2r-(mol_Pbr./2);
        mol_PbOp = mol_Pbr;

    elseif mol_Pbr > 2.*mol_O2r
        mol_Pbp = mol_Pbr - (2.*mol_O2r);
        mol_O2p = 0;
        mol_PbOp = 2.*mol_O2r;
    end

    %Use amount of air and lead to determine amount of water needed
    dhH2O = dhH2Op - dhH2Or;

    mol_H2O = (mol_Pbr.*dhPbr + mol_O2r.*dhO2r + mol_N2.*(dhN2r - dhN2p)...
        - mol_PbOp.*(-202.25 + dhPbOp) - mol_O2p.*dhO2p ...
        - mol_Pbp.*dhPbp)./(dhH2O);

    mdot_H2O = 18.01528.*mol_H2O./453.6; %lbs/s of water required

    plot(mdot_H2O,TF);
end

xlabel('Water Flowrate (lbm/s)');
ylabel('Chamber Temperature (F)');
legend('air = 0.5 lb/s','air = 1 lb/s','air = 2 lb/s','air = 3 lb/s','air = 4
lb/s');
%{

%Print important results to the screen
fprintf('\nFor a lead flowrate of %1.0f lbs/hr of lead,\n',mdot_Pb);
fprintf('and an accompanying air flowrate of %1.3f lbs/s of
air,\n',mdot_air);
fprintf('a water flowrate of %1.3f lbs/s is required,\n',mdot_H2O);
fprintf('to keep the reaction temperature at %1.1f F.\n\n',TF);

%}

%% Next Section is to physically design the injector.
mdotPb = 6000; %Mass flowrates of lead lb/hr
mdotair = 2; %Air flowrate lb/s
rhoPb = 665; %lead density lb/ft^3
pair = 2; %Air pressure psig
gam = 1.4; %Gamma for air
R = 1716; %specific gas constant ft-lbf/slug-R
Visc = .00175*.000145038; %psi-s
RhoAir = 0.082; %Atmospheric air density lb/ft^3

figure(2)
hold on
```

```
%Desiging the injector
for DeltaP = [30] %lead pressure psig

    vlead = sqrt(2*DeltaP*32.174*144/rhoPb); %lead speed ft/s
    Ainj = 144.*mdotPb./(3600.*rhoPb.*vlead); %in^2- jet injection area
    Dinj = sqrt(4.*Ainj./pi); %in- jet injection diameter
    Rinj = Dinj./2; %jet injection radius in
    alpha = 90; %Spray angle (deg)

    %Calculate constants used in Bazarov Equations
    a = tand(alpha/2)/(1+tand(alpha/2));
    sa = sqrt(a);

    phi = 0.0001;
    acount = 10;
    while acount > sa
        phi = phi + 0.001;
        acount = (1-phi)*sqrt(2)/sqrt(2-phi);
    end

    mu = phi.*sqrt(phi)./sqrt(2-phi); %Discharge Coefficient
    Anoz = Ainj./mu; %Nozzle area in^2
    Dnoz = sqrt(4.*Anoz./pi); %Nozzle diameter in
    Rnoz = Dnoz./2; %Nozzle Radius in
    A = sqrt(a)./mu;

    hfilmbar = 1-sqrt(1-phi);
    hfilm = hfilmbar.*(Dnoz./2); %in, thickness of film at nozzle

    n = 2; %Number of tangential inlets
    Rinb = [1.5]; %Empirical Constant
    Rin = Rinb.*Rnoz; %Radial Location of Inlet in
    Fin = (Rin.*Anoz)./(Rnoz.*A); %Total Injection area in^2
    Din = sqrt(4.*Fin./(n.*pi)); %Injection site diameter in
    Dvc = 2.*Rin + Din + 2.*.1/25.4; %Vortex chamber diameter  in
    Rvc = Dvc./2; %Vortex chamber radius in
    Lvc = 2.75 .* Din; %Vortex chamber length in
    Edge = Rin + Din./2; %Value used in early SMD calculations

    pair = 3; %Air pressure psig
    p0 = 14.7+pair; %Air pressure psia



    M = 0.002; %Mach number calculation
    while p0/14.7 > (1+(0.2*(M^2)))^(3.5)
            M = M + 0.002;
    End

    vair = M*sqrt(gam*R*(Tair*9/5)); %Air speed ft/s

    %Calculate SMD from Rizkalla and Lefebvre
```

```
    BOOK_SMD = ((3.33e-
3).*(sqrt(0.00251.*rhoPb.*(1/1728).*(hfilm./2).*32.174.*12)./(RhoAir.*(1/1728
).*vair.*12)).*(1+((mdotPb./3600)./mdotair))...
    + (13e-
3).*((((Visc.^2).*32.174.*12)./(0.00251.*(rhoPb./1728))).^0.425).*((hfilm./2)
.^0.575).*((1+((mdotPb./3600)./mdotair)).^2)).*25400;

%     plot(pair,BOOK_SMD);
    rhoair = 0.0709; %density of air (lbm/ft^3)
    D0 = BOOK_SMD; %average droplet diameter in microns
    D = 0.176.*((T./298).^(3/2)); %Mass diffusivity of O2 in air (cm^2/s)
    tb = (D0.^2).*((1/10000)^2).*rhoPb./(4.262*rhoair*D); %Burn Time
calculation s

    %With burn time use air speed to find length of combustor
    Pair = 16.7; %Air pressure in psia
    Mach = 0.001; %Calculate Mach number

    if Pair < 14.7
        disp('Gauge Pressure must be above 14.7 psi');
    else

        while 14.7/Pair < ((1+((gam-1)/2)*(Mach^2))^(-gam/(gam-1)))
            Mach = Mach + 0.001;
        End

        sonic = sqrt(gam.*T.*287) .* 3.28084; %sonic speed ft/s
        L_comb = sonic.*Mach.*tb; %Calculate combustor length ft
    %     fprintf('Droplet burn time is approimately %1.1f ms\n',tb*1000);
    %     fprintf('Droplet speed is approximately %1.1f ft/s\n',sonic*Mach);
    %     fprintf('This requires a combustor that is %1.2f ft
long\n',L_comb);
    End

    plot(mdotPb,D0);
end

%=( (0.00333)*(SQRT(0.00251*C17*(1/1728)*(C33/2)*32.174*12)/(0.082*(1/1728)*J
20*J21*12))*(1+((C5/3600)/C6))+
%(0.013)*((((C18^2)*32.174*12)/(0.00251*(C17/1728)))^0.425)*((C33/2)^0.575)*(
(1+((C5/3600)/C6))^2))*25400
xlabel('Lead Flowrate (lb/hr)');
ylabel('Droplet SMD (microns)');
%leadpress = legend('10 psig','20 psig','30 psig','40 psig');
airpress = legend('10 psig','20 psig','30 psig','40 psig');
%leadtitle = get(leadpress,'Title');
airtitle = get(airpress,'Title');
set(airtitle,'String','Lead Pressure');


%Print important dimensions of injector
fprintf('\nThe following are dimensions of the injector\n');
fprintf('Vortex Chamber length: %1.3f in\n',Lvc);
fprintf('Vortex Chamber diameter: %1.3f in\n',Dvc);
fprintf('Number of inlets: %1.0f\n',n);
```

```
fprintf('Diameter of inlets: %1.3f in\n',Din);
fprintf('Diameter of nozzle: %1.3f in\n\n',Dnoz);
```